Carbon and water cycle reconstructions across the Cretaceous-Paleocene boundary through plant wax lipids.

by

Robert Dylan Bourque

Department of Earth and Planetary Sciences

McGill University

Montreal, Quebec, Canada

August 2019

A thesis submitted to McGill University in partial fulfillment of the requirements of the degree of Master of Science

Abstract

The Cretaceous-Paleogene extinction has been one of the most heavily studied mass extinction events from the fossil record, with many aspects from the causation and effect of the extinction having been well studied, but with some areas still not having been explored in great detail. After an extended period of warming, there was a cooling event before the K-Pg extinction occurred that lasted for around 100,000 years, with the Chicxulub impact having been followed by a period of instability where plant communities were recovering. While these have been well studied, changes to the global carbon cycle remain uncertain and changes to the global water cycle have received little attention.

By studying the isotopic composition of plant wax lipids preserved in sediments from across the K-Pg boundary, it becomes possible to put together a clearer image of how the carbon and water cycles were behaving up to and across the mass extinction event. These sediments were collected from southern Saskatchewan, Canada, with the lipids having been extracted from the sediments and had the abundance of individual lipid chains and isotopic compositions of hydrogen and carbon measured. Modern plant wax fractionation was used as a basis to relate the isotopic values back to the expected values of atmospheric CO_2 and rain water, providing a baseline for the carbon and water cycles and observing how they change across time. Inferences on these cycles show the region was characterized by isotopically light rain water but with no long term trends in water isotope composition, while carbon values show cyclicity reminiscent of Milankovitch orbital cycles, with neither isotope record showing long term effects caused by the extinction, suggesting a relatively rapid recovery of within 10,000 years for both cycles.

Résumé

L'extinction crétacé-paléogène est l'un des phénomènes d'extinction de masse les plus étudiés parmi les archives fossiles. De nombreux aspects de la cause et de l'effet de l'extinction ont été bien étudiés, mais certaines zones n'ont pas encore été explorées de manière très détaillée. Après une longue période de réchauffement, il s'est produit un refroidissement avant l'extinction de la K-Pg qui a duré environ 100 000 ans. L'impact du Chicxulub a été suivi d'une période d'instabilité pendant laquelle les communautés végétales se rétablissaient. Bien que ceux-ci aient été bien étudiés, le cycle du carbone n'a été exploré que par des méthodes limitées et le cycle de l'eau encore moins.

En étudiant la composition isotopique des lipides de cire végétale conservés dans les sédiments situés au-delà de la limite K-Pg, il devient possible de donner une image plus claire de la façon dont les cycles du carbone et de l'eau se comportaient jusqu'à l'événement d'extinction de masse. Ces sédiments ont été collectés dans le sud de la Saskatchewan, au Canada, les lipides ayant été extraits des sédiments et l'abondance de chaînes lipidiques individuelles et de compositions isotopiques d'hydrogène et de carbone a été mesurée. Le fractionnement moderne des cires de plantes a servi de base pour ramener les valeurs isotopiques aux valeurs attendues de CO2 atmosphérique et d'eau de pluie, en fournissant une base de référence pour les cycles du carbone et de l'eau et en observant leur évolution dans le temps. Les inférences sur ces cycles montrent que la région est inondée d'eaux de pluie isotopiquement légères mais sans tendance à long terme, tandis que les valeurs de carbone montrent une cyclicité rappelant les cycles orbitaux de Milankovitch, aucun enregistrement isotopique ne montrant des effets à long terme causés par l'extinction, ce qui suggère une reprise relativement rapide de 10 000 ans pour les deux cycles.

Preface

The thesis presented here is the culmination of the author's original research at the Earth and Planetary Science Department of McGill University from 2017 to 2019. The article is intended to be submitted for review for the purpose of submission to complete the author's Master's degree in the program, where the author is the primary contributor and Peter Douglas is the author's primary supervisor, with Hans Larsson as the co-supervisor.Sample preparation, data analyses, and inference were conducted by the author under the guidance and supervision of Peter Douglas while the field work was performed under the supervision of Hans Larsson.

Acknowledgements

I would first like to thank my supervisor, Peter Douglas, for taking me under his wing and giving me this opportunity to do this research project, for all his guidance and support over the past two years. I would also like to thank my co-supervisor, Hans Larsson, for aiding me with the field work portion of my project and for providing his expertise on the time period that was looked at for this project. I would also want to thank my parents and sister for their continual support for me to progress in my desired career.

I also have several very special individuals who were invaluable in helping me at various stages of my research and whom without this never would have been possible. Firstly, I would like to thank Emily Bamforth from the Royal Saskatchewan Museum's T.rex Discovery Center, whose expertise in the local region where I did my field work was invaluable and was an incredible help at various stages through my field work. A huge thank you to my field assistants who had volunteered to stay with me during the field season of 2018 to collecting and identifying the samples, which would be Aidan Olivier Howenstine, Tony Smith, and Claudia Selles. I also have to thank Hallie Street who was working with Emily during the summer of 2018 and was also an aid in the field work for that summer, as well as Alexandre Demers-Potvin who had aided at several points through that field season as well. A very special thanks to Thi Hao Bui, the head lab technician for Peter's lab that an invaluable aid in maintaining the equipment and maintaining the lab in top order. I also have a special thanks for Agnieszka Adamowiscz-Walczak who had aided me with the sample preparation at UQAM University and ran the analyses there that were essential for providing data to this thesis. I also have a special thanks to my fellow student Benjamen Keenan who was a huge help in the beginning of my Master's and

helping to teach me the methods for several of the procedures that were necessary for this project.

Finally, I would like to thank my other lab mates Regina Gonzalez, Robert Bogue, Ying Ran Lin, Emerald Stratigopoulos, and Jenni Ni for their continued support and friendship over the past couple of years.

Table of Contents

List of figures

List of Tables

Chapter 1: General introduction

The Cretaceous-Paleogene (K-Pg) boundary is the most recent mass extinction event in Earth's history and has been the most heavily studied, now known to have been linked to an asteroid impact that landed in the Gulf of Mexico (Hildebrand et al., 1991). The extinction wiped out 75% of all plant and animal species on Earth, with terrestrial and marine ecosystems being heavily affected by the impact (Norris et al., 1999; Labandeira et al., 2002; Vajda et al., 2001; Wolfe & Upchurch, 1986). Evidence for an asteroid impact has been found globally and ranges from direct evidence within the Chicxulub crater and indirect evidence from the aftermath of the impact, which include tektites in regions near the impact site, shocked quartz associated with the high forces of the impact, and a layer of iridium-rich clay that has been found globally in terrestrial and marine deposits and is used to mark the boundary between the Cretaceous and Paleogene (Alvarez et al., 1980; Smit & Hertgen, 1980). The Chicxulub crater is in the subsurface on the Yucatan peninsula off the coast of Mexico, with an estimated of diameter of 180 to 200 km that, at the time of impact, would have landed in carbonate rich continental marine deposits. A range of hypotheses has been put forth on the effects such an impact would have caused to the global system, none mutually exclusive from each other, which have ranged from the release of a large enough volume of aerosols to create an extended period of darkness (Pope et al., 1994), short term global cooling (Vellekoop et al., 2014; Vellekoop et al., 2015), and long-term warming (Kaiho et al., 1999). There also would have been more immediate effects that would have devastated the Americas and possibly have been more widespread as well, including earthquakes from seismic activity traveling through the Earth (Ivanov, 2005), large scale wildfires (Kring & Durda, 2002; Vajda et al., 2001), ejecta from the impact falling back down to the surface (Croskell et al., 2002), global production of acid rain which would damage

vegetation and calcareous shelled organisms (Prinn & Fegley jr, 1987), and the blast that would have occurred in the immediate vicinity of the impact site (Pope et al., 1997).

Although it is largely undisputed that the bolide impact was one of the primary forces behind the K-Pg mass extinction, the matter is complicated by the occurrence of the Deccan traps, a series of flood basalts, that were active around the time of the impact in India (Washington, 1922). This has been the source of debate for some time as it is unclear whether the Deccan traps had played a role in the K-Pg extinction event, with some studies concluding that they were the primary driver in the extinctions (Font et al, 2016; Petersen et al., 2016; Schoene et al., 2019) while other studies suggest the volcanism only played a minor role or even had no serious environmental effects in the over all stability of ecosystems before the impact based on studies showing no dramatic changes in diversity before the impact (Chiarenza et al., 2019; Sheehan et al., 2000). The flood basalts are suggested to have been a driver in the Cretaceous-Paleogene mass extinction as flood basalts have been linked to other mass extinctions in the Earth's past (Clapham & Renne, 2019). The main issue in the debate results from the scarcity of studies with adequate sample sizes right before the impact to study changes in ecosystem diversity, along with conflicting climate models and even the timing of the Deccan eruptions (Fig. 1). The number and timing of eruptions are disputed due to the inconsistent results from studies that use different methods of dating the pulses of eruptions, including U-Pb zircon geochronology and argon-40/argon-39 isotope dating. These widely different timings in eruptions cause conflicting conclusions to be put forth regarding when the eruptions occurred and their duration based on the methods used (Schoene et al., 2019; Sprain et al., 2019).

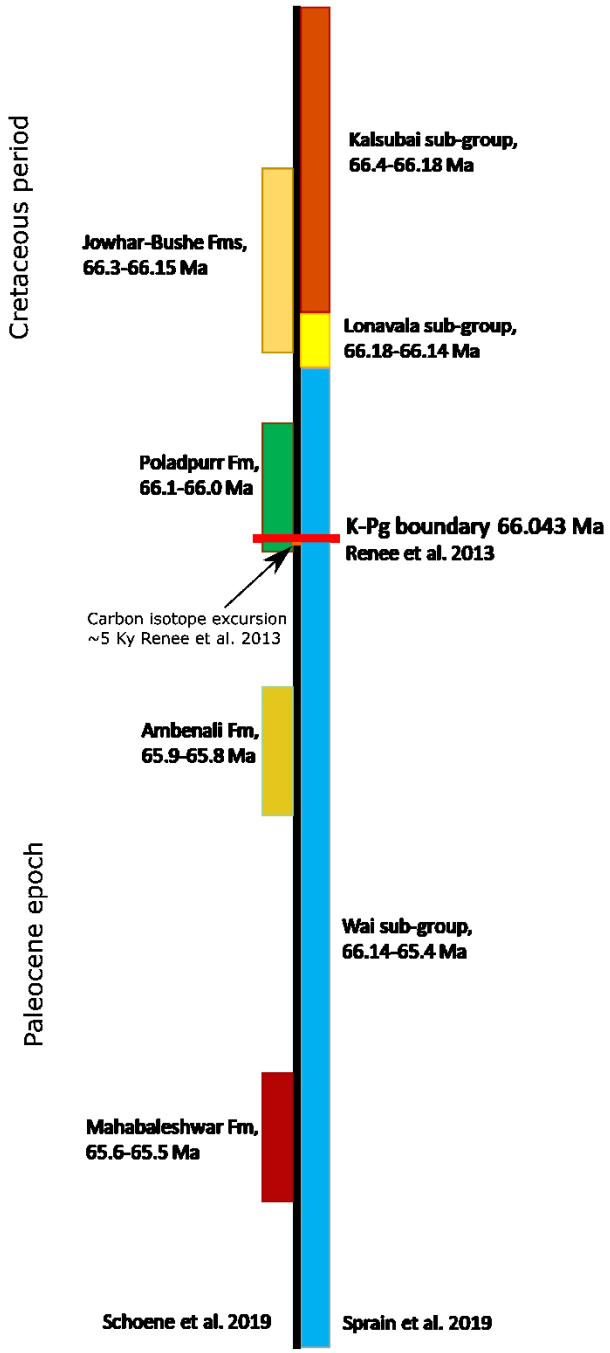

246

247 Figure 1: Sequence of major events around the K-Pg boundary, including the boundary itself, the carbon isotope

248 excursion, and the potential Deccan Trap eruptions based on two different studies to showcase the conflicting timing

249 intervals.

The biggest disputes as a result of these mixed findings on the Deccan traps has revolved around the idea of the extinction having started before the bolide impact as several environments, both terrestrial and marine, were said to have been experiencing a loss in overall diversity prior to the boundary, with links having been made to global climate change due to the active volcanism based on a cooling event leading up to the boundary (Peterson et al., 2016). This cooling occurred within the last 0.1 million years leading up to the boundary and followed several million years of global warming (Wilf et al., 2003). Cooling is linked to short term effects after large volcanic events as a result of sulphate aerosols being released into the atmosphere and reflecting solar radiation, though they only remain in the atmosphere for around two years (Bradley, 1988; Khadkikar et al., 1999; Saxena et al., 1997).

In addition to long term trends in temperature, there is evidence for cyclical variations in humidity in terrestrial settings, alternating from drier, semiarid to more humid conditions in more temperate climates (Lehman, 1989). These trends are associated with Milankovitch cycles, which are changes in the Earth's orbit with each factor being affected on different time scales, which include the Earth's precession over 21,000 year time scales, obliquity over 41,000 years, and eccentricity over shorter 100,000 and longer 400,000 time scales. These orbital cycles have been recorded predominately in marine strata from this time period (MacLeod et al., 2001; Isaza-Londoño et al., 2006; Westerhold et al., 2008) but are rarely recorded in terrestrial settings. Despite the claims for increased rates of extinction due to changing climates, some recent papers have shown that this may not be the case, with marine records showing they maintain diversity up to the boundary with no notable loss in overall diversity (Sepúlveda et al., 2019). Terrestrial records, on the other hand, may be affected by a preservation bias rather than a genuine loss in

diversity being observed given the much more limited sites of terrestrial fossils from just before the impact (Chiarenza et al., 2019).

The carbon and water cycles across the boundary

A question that remains unsolved is how the carbon and water cycles were affected by the bolide impact, as it would be expected that a large bolide impact and extinction event would have global effects on biogeochemical cycles, but these effects are poorly constrained. Furthermore, due to the uncertain nature of the timing of the Deccan trap eruptions and correlating the eruptions with inferences made on global climate before the Chicxulub impact, knowing the exact effects that volcanism had before the impact is also unclear (Jerrett et al., 2015). Previous studies have looked at the bulk organic carbon record at the boundary, as one of the defining features of the K-Pg extinction is a pronounced negative carbon isotope excursion above the boundary (Arens and Jahren, 2000). Although this has proved useful for identifying the boundary and associating the iridium rich layer with an increase in the oxidation of organic matter (Meyers & Simoneit, 1990), it does not sufficiently resolve the large number of processes that could have altered the global carbon cycle. The isotopic signal of bulk organic carbon is a complex mixture of multiple carbon-cycle processes as it represents a signal of all the organic carbon present in a system, including biological and sediment derived carbon, which does not provide a perfectly accurate account of atmospheric conditions. So far the most informative work on the carbon cycle from around the time of the impact has come from marine records, where studies have shown a decoupling of the deep water column and closer to the surface ocean carbon cycles, resulting in the complete inability for nutrients to be cycled through the water

column, which has been estimated to last hundreds of thousands of years (D'Hondt et al., 1998, Alegret et al., 2009). This shutdown of the vertical water column has been attributed to a prolonged collapse of the biological pump; however evidence has shown that primary productivity may have recovered quickly, suggesting some other factor must explain the delay in the recovery of the carbon cycle within the oceans (Alegret et al., 2009). Additionally, some groups of planktonic organisms show evidence of having recovered quickly from the extinction (Alegret et al., 2012) in a similar manner to the recovery of terrestrial systems (Vajda et al., 2001). In contrast with the relatively detailed studies of the carbon-cycle change, there have not been any studies that have focused on the effects the impact had on the water cycle.

Plant wax lipids

This lack of clarity in regards to the water and carbon cycles at this crucial period in Earth's history thus warrants a rather novel method for investigating the time period in more detail. One such method is available through the study of plant wax lipids. Plant waxes, also known as epicuticular waxes, are formed on the leaves of plants as a means of protecting the plant from disease, ultraviolet radiation, and water loss (Kolattukudy, 1969). The waxes are primarily composed of straight-chain aliphatic hydrocarbons, including long-chain *n*-alkanes which are the target of our isotopic analysis. The carbon that makes up the lipid chains is proximally sourced from atmospheric CO_2 that is taken in from photosynthesis (Fig. 2), while the hydrogen molecules are derived from water that is taken up by the roots of the plant (Fig. 3), with both of the atoms going through a myriad of biosynthetic processes before being incorporated into plant waxes. (Sachse et al., 2012; Diefendorf & Freimuth, 2017). This

combination of sources means that the isotopic ratio of plant waxes is largely controlled by the isotopic composition of atmospheric CO_2 and rain water at the time the waxes were produced, although there are other environmental variables that can influence these values.

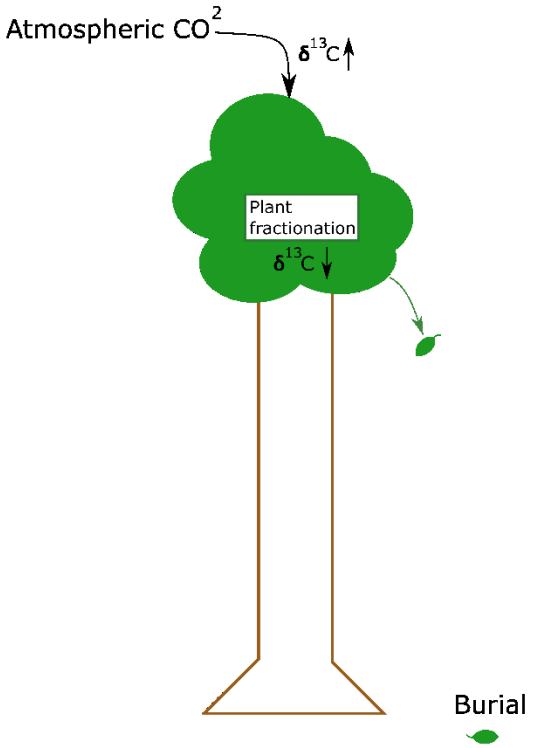

Figure 2: The process from which CO^2 is extracted from the atmosphere from photosynthesis and then incorporated into leaf waxes through plant fractionation, before leading to burial of the plant and the wax coating. Also shown are the affects of each step in the process on the isotopic ratio of carbon.

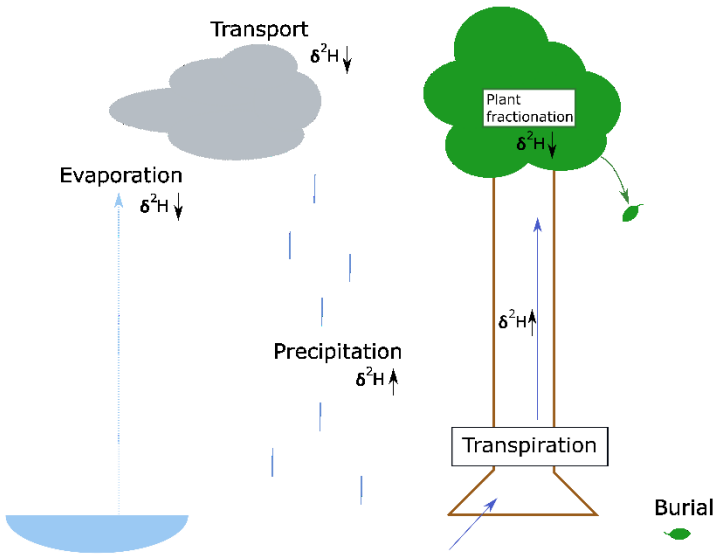

Figure 3: The process from which water is transported and taken up into plants where the hydrogen is incorporated into the leaf wax structure before burial of the leaf waxes. Also indicated are the affects each step has on the isotopic composition of hydrogen.

Two factors that affect the isotopic ratios of both carbon and hydrogen would be the types of plants producing the leaf waxes and if they are terrestrial or aquatic. Previous studies have noted that different species of trees sharing the same habitat can have remarkably different hydrogen isotopic ratios in the plant waxes they produce despite inhabiting the same ecosystems, with differences sometimes reaching as much as 100‰ (Sachse et al., 2012). These extreme differences could then affect the ratio observed in the sediments if there are dramatic shifts in the dominant flora in a given ecosystem. The isotopic ratios of carbon and hydrogen can be affected in a few ways independent of climate, most notably by hydrological changes with different species of plant reacting differently to changes in hydrology, influencing the isotopic ratio of carbon isotopes (Diefendorf & Freimuth, 2017). However in this study hydrogen isotopes measurements provide a framework for changes in the water cycle to take into consideration.

Hydrogen isotopes are also affected by evaporation in the soil, as evaporation preferentially selects for lighter isotopes and results in a larger isotopic ratio when taken up by plants (Sachse et al., 2012). This is taken into account when examining the different chain lengths of the plant waxes, as high levels of evaporation would strongly affect terrestrial but not aquatic plant wax lipids, and so comparing how the isotopic ratios of both lipid chains behave can help resolve if a large degree of evaporation was occurring or not at the time of leaf wax formation. Additionally, fractionation occurs during the process of leaf wax formation, which alters the isotopic ratio observed in the waxes from the original source of the molecules; however, the original ratios can still be calculated and so inferences on the climate can still be made. The type of carbon fixation used by plants can also have a large affect on carbon isotopes, as C4 carbon fixation results in much higher fractionations than in plants that go through C3 fixation (Diefendorf & Freimuth, 2017). This is unlikely to affect the studied sediments as our data does not show evidence for C4 plants being present (as will be discussed later), and becauseC4 plants were not widespread at the end of the Cretaceous (Osborne & Beerling, 2005). In addition to the type of fixation plants use, the length of these hydrocarbon chains are also produced in different quantities, with aquatic plants producing low to mid length lipid chains, most notably in this study C_{23} and C_{25} while terrestrial plants produce longer length lipid chains, with this study focusing on C_{29} (Ficken et al., 2000; Aichner et al., 2010). As C_{27} is produced in intermediate quantities by both aquatic and terrestrial plants, it could potentially provide information on whether aquatic or terrestrial plant waxes are more abundant in the samples collected, with comparisons between the aquatic and terrestrial hydrocarbons providing a greater degree of information on how both systems could have changed through time and how they were affected.

363 The isotopic composition of atmospheric CO_2 reflects the sources and sinks of the gas as
364 different sources and sinks have different isotopic fractions. These sources include surface
365 oceans, volcanism (which have an isotopic composition similar to the mantle), sedimentary
366 deposition and erosion, and terrestrial biota (Sharp Z. D., 2007). With each source/sink having its
367 own isotopic signature, it is possible to relate changes observed in the atmospheric composition
368 of carbon to changes in these reservoirs and sinks, with sources that differ more strongly from
369 the isotopic composition in atmospheric CO_2 having an overall larger effect relative to the
370 change in the carbon reservoir (Diefendorf et al., 2017). As such, volcanic input into the
371 atmosphere is weak due to the small contribution of CO_2 from volcanic releases coupled with the
372 similar isotopic signal (Mason et al., 2017), along with chemical weathering playing a small role
373 in influencing atmospheric carbon as a result of the contribution of CO_2 to the production of
374 HCO_3 being small (Fig. 4), only around 1‰ (Mook et al., 1974). Oceanic and terrestrial
375 contributions to atmospheric CO_2 have different residence times (IPCC, 2005), with oceans
376 having longer residence times due to CO_2 being drawn down to the ocean floor and buried
377 (Ittekkot, 1993). This is noteworthy due to the known shutdown of ocean to atmosphere sink
378 after the K-Pg mass extinction (D'Hondt et al., 1998, Alegret et al., 2009), which would have
379 limited the removal of CO_2 from the atmosphere after the extinction event and would have
380 resulted in a depletion of the carbon isotopic signal in the atmosphere as there would be a build
381 up of lighter carbon isotopes in the surface ocean. An additional source of carbon isotopes on the
382 atmosphere would be from the burial of carbon (Meyers 1994) and respiration from microbes,
383 with burial showing to be a strong sink for isotopically heavy carbon while respiration releases
384 larger quantities of isotopically heavy carbon (Sharp, 2007).
385

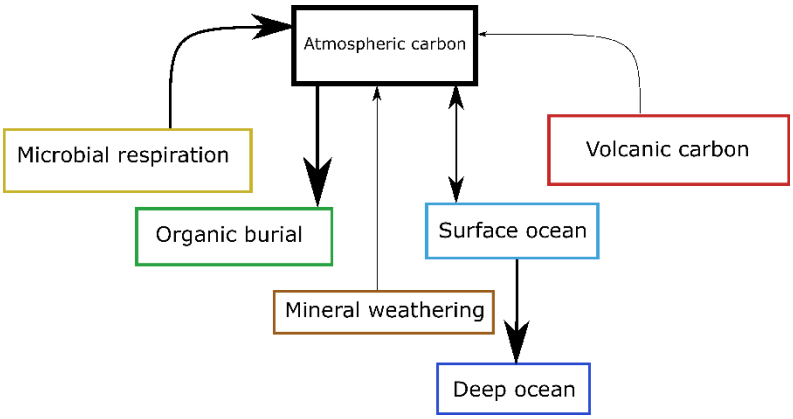

Figure 4: Simplified model showing the flow of carbon to and from the atmosphere, with the size of the arrows representing the relative strength and directional flow of atmospheric carbon.

As the isotopic composition of carbon in the plant waxes largely reflects the isotopic composition of carbon dioxide, this makes the lipids excellent markers for observing changes in the global carbon cycle across the K-Pg boundary. Carbon enters the atmosphere through several notable sources that could influence the isotopic composition of atmospheric carbon, which include: Mantle derived CO_2 which is released through volcanism, surface ocean exchange, and the sequestering and decomposition of terrestrial biota most likely having the largest influence on the atmospheric carbon isotopic composition, with a special note for siliciclastic weathering which is thought to have been a factor to consider with increased volcanism (Schoene et al., 2019). The reason that organic carbon has the largest effect and would be the most likely to cause noticeable changes in the signal is due to the highly negative $\delta^{13}C$ signal, with terrestrial biota having an isotopic ratio of -23‰ compared to the -7‰ signal from atmospheric values (Sharp Z. D., 2007). This results in terrestrial biota having a greater influence on the atmospheric carbon isotope values with smaller change needed. Due to the nature of these plant waxes, they can inform the climatic conditions and primary contributors to atmospheric CO_2 in Earth's past.

Hydrogen isotopes of meteoric water, by contrast, reflect a range of atmospheric conditions related to precipitation, which include the distance traveled from the original source of water vapour, the fraction of water vapour that has already precipitated, temperature, and humidity (Sachse et al., 2012). This combination of factors means that the hydrogen isotopes reflect a more localized signal, providing an indicator of local regional hydrology. However, hydrogen isotopes derived from precipitation do typically change on a global scale during global climate changes, and changes in the local hydrological cycle can be used to infer larger scale global changes (Feng & Epstein, 1994). Additionally, observing long term trends and changes as well as the values of the hydrogen isotopes can help give an idea of the background climate variability, with the local changes in the hydrological cycle reflecting greater global conditions and their behavior before and after the impact. The hydrocarbon chains of plant waxes provide information as they are produced at different lengths, identified by the number of carbons present in a chain with plants primarily producing hydrocarbon chains with an odd number of carbon molecules present.

The reason these lipids are relevant to this kind of research is that they remain intact in sediments so long as catagenesis had not occurred. Catagenesis is the process of breaking down organic matter into hydrocarbons through cracking, which breaks apart the lipid structure. Additionally, lipids are preserved in a variety of sediments and do not require specific depositional environments to be present nor the fossils of plants or even amber, the only caveat being their abundance which is generally linked to the abundance of total carbon in the sediment (Sachse et al., 2012; Diefendorf et al., 2017). While this is not the first study to look at plant wax lipids across the K-Pg boundary (Yamamoto et al., 2010), it is the first to look at in-situ plant wax lipids in a terrestrial setting. Yamamoto et al. (2010) investigated plant waxes collected

from marine sediments near Cuba that were blown in from Northern Africa, with the authors having noted that based on the trends in the carbon isotopic record that hydrological conditions and changes in plant composition were influencing these values, however as the study only looked at carbon isotopes, my study has the advantage of looking into hydrological changes in greater detail. The motivation behind using this method of isotope analysis was that it has never been done across the Cretaceous-Paleogene boundary with in-situ sediments before, making it an ideal opportunity to test a novel method of study over a well explored event in the geological past. Plant wax isotopes are unique in that they provide a clear reading of the isotopic signal of atmospheric carbon and hydrogen from precipitation, something that many other methods of recording isotopic measurements are unable to isolate, often resulting in mixed signals that are subject to outside influences and do not provide a pure signal.

Chapter 2: Plant wax isotope analysis from southwestern Saskatchewan, Canada

Robert Bourque[1], Peter Douglas[1], Hans Larsson[2]

[1] Department of Earth and Planetary Sciences, McGill University, 3450 University Street H3A 0E8, Montreal, Quebec, Canada.

[2] Redpath Museum, McGill University, 859 Sherbrooke Street West H3A 0C4, Montreal, Quebec, Canada.

Abstract

The Cretaceous-Paleogene (K-Pg) mass extinction is the most recent mass extinction in the geologic record and is one that has been heavily studied and debated for decades, with a large focus on whether or not the extinction occurred before the Chicxulub impact as a result of environmental change. Additionally, there has been a large focus on the recovery after the extinction and how long it took for ecosystems to recover and stabilize. In this study we measure the isotopic ratios of carbon and hydrogen extracted from plant wax lipids found in sediments spanning the K-Pg boundary from Saskatchewan, Canada, inferring changes in the carbon cycles respectively across this period to better understand how these systems were behaving before and after the impact. Plant wax lipids were isolated from the parent sediments with the relative abundance of different chain-length lipids measured along with $\delta^{2}H$ and $\delta^{13}C$ isotopic measurements taken from each sample. Inferences made on changes to the carbon and water cycles were then subsequently compared to previous studies on post-impact ecosystem recovery and climate to see how the cycles were reacting on the order of 10,000+ year timescales. $\delta^{2}H$

showed no clear signal across the boundary with fluctuating signals across the different types of lipid chains with a long term decrease in δ^2H found at both sections. The most notable feature from the hydrogen record is their highly negative nature (-100 to -180‰) in comparison to what is expected of these types of plants, indicating ^2H depleted precipitation likely as a result of orographic uplift over the Rocky Mountains. $\delta^{13}C$ measurements show cyclic variations across the boundary that are consistent across different lipid chains and for both localities with a range of 2‰. Two distinct cycles being noted, one with an inferred period of 100,00 years and another of 55,000 years, are interpreted here to be tied to Milankovitch cyclicity. The records for both carbon and hydrogen also lack any sign of a disruption as a result of the impact above the boundary, which indicates that both the carbon and water cycles recovered within 16,000 years, with the carbon cycle specifically resuming cyclic variability observed before the impact.

2.1 Introduction

The Cretaceous-Paleogene (K-Pg) boundary is the most recent mass extinction event in Earth's history, known to have wiped out 75% of all plant and animal species on Earth (Norris et al., 1999; Labandeira et al., 2002; Vajda et al., 2001; Wolfe & Upchurch, 1986). The primary driver of the extinction event is linked to an asteroid impact (Hildebrand et al., 1991). However, the matter is made a bit more confusing with evidence of large shifts in global climate (Wilf et al., 2003; Peterson et al., 2016) along with the Deccan Traps (Washington, 1922), a series of flood basalt volcanism, occurring across the K-Pg boundary in India (Schoene et al., 2019; Sprain et al., 2019). With the Deccan Trap volcanism having been linked as early influencers to the K-Pg mass extinction, with the Chicxulub impact not acting as sole driver (Schoene et al.,

2019). Much work has been done on the effects the impact would have had on the planet (Pope et al., 1994; Kaiho et al., 1999; Vellekoop et al., 2014; Vellekoop et al., 2015) as well as it's effect on the carbon cycle (Arens & Jahren, 2000; Therrien et al., 2009) with one of the primary focuses being on bulk carbon isotopic measurements ($\delta^{13}C$) to infer changes in atmospheric CO_2. While these measurements have proven useful for identifying the boundary, it remains unclear what observed changes in carbon isotopic ratios indicate in terms of global carbon cycle changes as a result of the impact.

The objective of this study was to perform measurements of plant wax lipid distributions and carbon and hydrogen isotopes, alongside measurements of bulk carbon isotopes, across the K-Pg boundary to infer changes to the carbon and water cycles before and after the impact. Other goals were to better understand changes in plant ecology across the extinction events and to compare the results from plant wax stable isotope measurements to more conventional isotope measuring techniques for this time period.

In this study, carbon and hydrogen isotopes were derived from the hydrocarbon chains that make up plant wax lipids, which source carbon from atmospheric CO_2 and hydrogen from rain water, making them prime candidates for inferring environmental changes (Sachse et al., 2012; Diefendorf & Freimuth, 2017). The samples used in this study were taken from a pair of sites in southern Saskatchewan, Canada, notable for the distinct and excellent preservation of the K-Pg boundary. Based on inferences made using modern plant waxes as a basis, this study looks into how the carbon and water cycles dehaved during the final hundred thousand years of the latest Cretaceous and how they behaved following the Cretaceous-Paleogene mass extinction. In addition to plant wax stable isotope measurements, more general measurements of organic carbon and $\delta^{13}C$ were taken for the purposes of comparing with previous studies. Before the

impact, the climate was in the midst of a cooling event in the last 100,000 years of the Maastrichtian (Peterson et al., 2016), which is often linked to the Deccan trap volcanism that was occurring over this time period as an early driver of extinctions before the impact (Peterson et al., 2016). Constraints on ecosystem recovery (Lomax et al., 2001; Maruoka et al., 2007) provided a framework to compare these results to in order to have a better understanding of carbon and water cycle behavior, as plant communities recovered in a fairly short amount of time, taking as little as 10,000 years to recover. We also examine the potential for Milankovitch-scale climate and carbon-cycle variability, since orbital variations have been inferred to have played a significant role in late Cretaceous global climates (MacLeod et al., 2001; Isaza-Londoño et al., 2006; Westerhold et al., 2008) and thus would have an influence on the carbon and water cycles.

2.2 Study Area

2.2.1 Localities

The study area consisted of two localities in southern Saskatchewan: Chambery Coulee and Highway 37 (Fig. 5). These sites were chosen due to the exceptional preservation of the K-Pg boundary (McIver et al., 2002; Bamforth et al., 2014; Jerrett et al., 2015; Redman et al., 2015) as well as for the presence of sedimentary units of the uppermost Frenchman and lowermost Ravenscrag formations (Fig. 6), allowing for a continuous study across the boundary marking the extinction event. The Frenchman Formation is a unit of latest Cretaceous age that is contiguous with the Hell Creek Formation of Montana due to both formations having similar fauna and being composed of latest Cretaceous sediments leading up to and including the K-Pg boundary, with the Frenchman being composed of sand and clay lithesome units which alternate throughout

the formation (Kupsch, 1957). The Ravenscrag Formation earliest Paleocene in age and predominantly composed of silt. It is distinct for beginning with the Ferris coal seam, a coal seam present above the iridium-rich clay layer (McIver, 1989). The K-Pg boundary is a thin clay layer that is rich in iridium and has been interpreted as being the fallout of an asteroid impact, marking the upper boundary of the Frenchman Formation as well as other contemporaneous formations (Alvarez, 1980). The Cretaceous-aged rocks of western Canada were notably not deeply buried or heated (Walls et al., 1979), which implies good potential for preservation of the plant wax *n*-alkanes applied in this study.

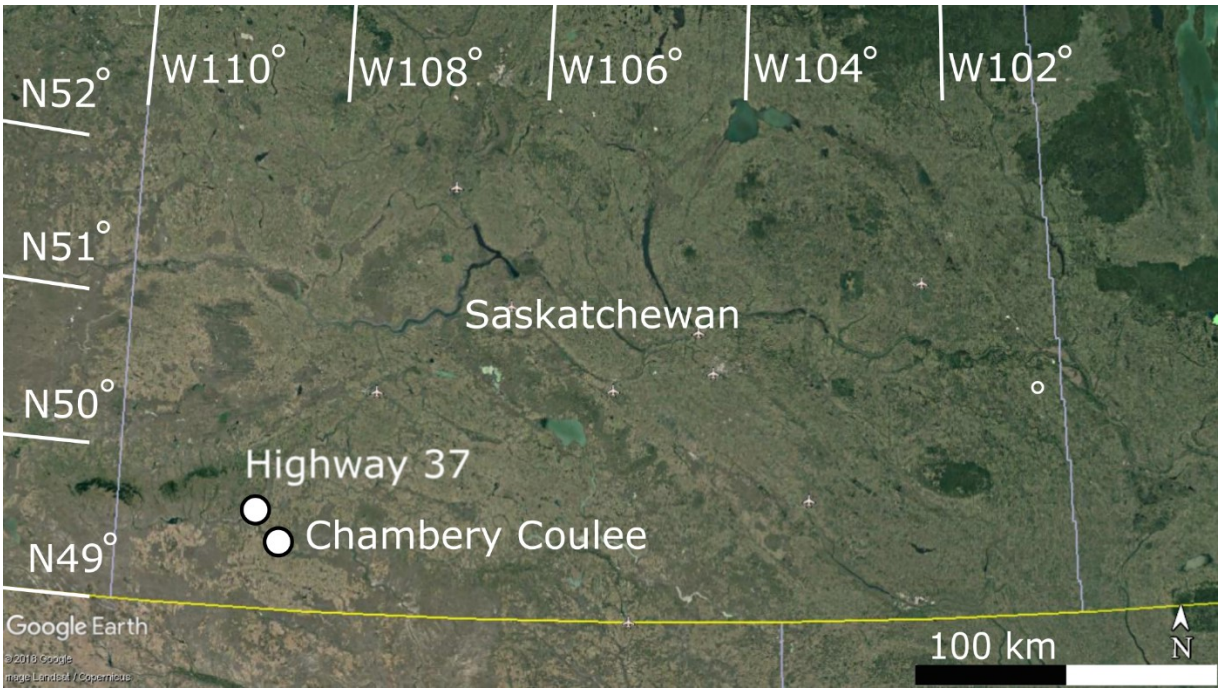

Figure 5. Map of southern Saskatchewan with the field sites for Highway 37 and Chambery Coulee marked. Photo taken from Google Earth Pro.

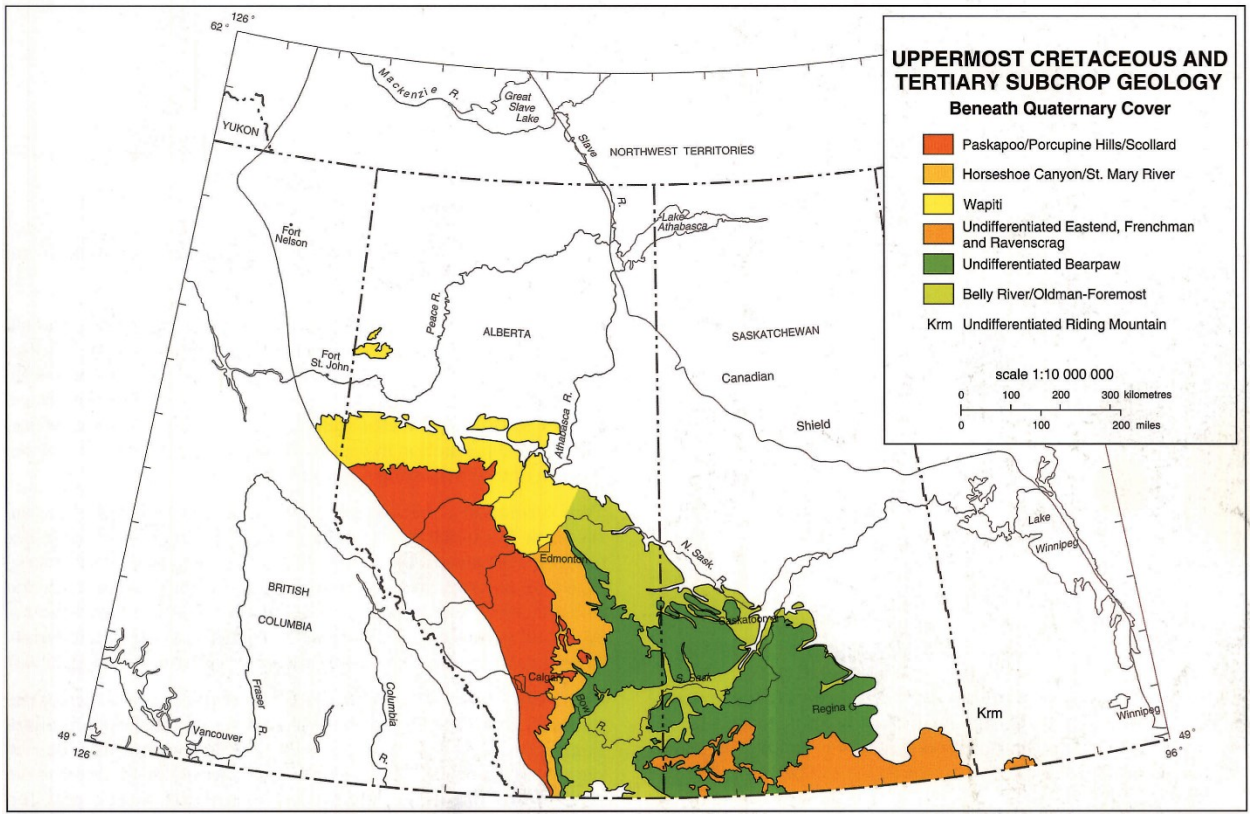

Figure 6: Geological map of southwestern Canada with a focus on late Cretaceous to Paleocene strata along the plains (Dawson, 1994).

The site at Chambery Coulee (Fig. 10 c) is a relatively small exposure on private property, with the exposure extending down a slope leading into the Frenchman River Valley near a dirt road, allowing for easy access. The site has over 30 meters of exposed strata with around 6 meters of the lowermost Ravenscrag overlying the Frenchman Formation, which can be up to 35 meters thick in some areas. The site of Highway 37 (Fig. 10 b) is a recently exposed outcrop that was uncovered during the construction of the highway it is named after, about 20 km south from Shawnovan, SK. It is notable in that the K-Pg section at this site is distinct and has had little weathering due to the recently exposed nature of the site. The site is also proximal to Chambery Coulee, located only 28.5 km from the Highway 37 site, offering the opportunity to compare geographically proximal strata. The section is only 18 m thick with around 9 meters of

strata from both formations being exposed, with the top of the section being capped by Quaternary glacial till. These sites were chosen due to the well exposed nature of the K-Pg boundary (Fig. 10 a) and good selection of strata for collection.

2.2.2. Stratigraphy

Chambery Coulee is the larger section that was visited, with the entire section explored nearly 35 meters thick (Fig. 7 b, Fig. 8 b). The bottom-most facies that was identified from the locality was an unconsolidated fine-grained siltstone that was around 150 cm in thickness, overlain by a uniform claystone that stretched for 395 cm. Overlying the claystone is another facies of fine-grained siltstone that was 110 cm thick, with a claystone that is a dark brown in colouration and around 30 cm in thickness overlying the siltstone, with the dark colouration suggesting the sediments to be more organic rich. This is overlain by a 20 cm thick layer of iron-rich claystone, giving off an orange colouration from the oxidized iron in the sediment. The next facies up starts as a siltstone before gradually transitioning into a claystone over 30 cm, with the top of the facies also being organic rich with dark sediment. The following facies is a claystone with a distinct mint-green colouration that is 100 cm in thickness. The next facies up is a fine grained brown siltstone that is 95 cm thick, transitioning into darker, organic rich matter at the top of the facies that is 120 cm thick. The sediment then transitions into organic poor siltstone for 260 cm with no change, though it then transitions into organic rich siltstone once more for 30 cm. The next facies up consisted of unconsolidated claystone for 500 cm, where it transitions from finer, consolidated claystone at the base upwards to more unconsolidated sediment. The next layer up was a 30 cm thick facies of dark brown siltstone that was notable for cleaving in almost horizontal layers, with a 70 cm thick layer of more yellowish siltstone overlying it that lacked the laminations visible in the darker siltstone beneath it. A fine-grained claystone unit was

the next up the sequence, once again unconsolidated and dark brown and stretched for about 585 cm into another very fine grained, yellowish siltstone that stretched for 440 cm. Above this facies is the K-Pg boundary, the base of a pink coloured very fine claystone that was 2 cm. Above the clay layer is the Ferris Coal seam, which at this site is 20 cm thick and is rich in plant matter. Overlaying the Ferris Coal seam is a silty grey claystone that is 10 cm thick before transitioning into a brown coloured claystone that is otherwise identical in grain size that is 6 cm thick. This is then superimposed with a thin layer of very fine black siltstone for 6 cm before the facies is replaced with a claystone, the very base of which is organic rich, which is approximately 200 cm thick. The rest of the sequence, around 250 cm thick before going into glacial till, is unconsolidated siltstone with various grain sizes, with occasional patches that are organic rich, and one spot that contained plant fossils 410 cm above the boundary.

Highway 37 is a smaller section but with more distinct facies than at Chambery Coulee, with the entire section being around 14 and a half meters in total thickness (Fig. 7 a, Fig. 8 a). The base of the section is a muddy siltstone that is a mixture of dark brown and light grey sediment that is around 3 meters in thickness from the point where it is visible from the top soil. This is superimposed by a facies of siltstone that is more uniform than the layer below and only 75 cm thick. Overlying this facies is a fine grained, organic rich siltstone that is 50 cm thick, followed by a fine grained siltstone that is yellowish brown in colour and contains small sulphur balls throughout the facies with a total thickness of 80 cm. Over this layer is an organic rich siltstone that is very similar to the facies below the underlying sulphur rich layer, though only 40 cm thick. The next facies up is a siltstone that is blue-green in colouration, likely a result of wearing on the sediments, which was around 165 cm in thickness. This is overlain by claystone

602 that is organic rich in the upper part of the facies but contains plant fossils in the lower portion,
603 with the entire facies being around 22 cm in thickness. The K-Pg boundary then overlies this
604 facies, once again thin at only 1 cm as with Chambery Coulee, before being overlain by the
605 Ferris Coal seam which is 16 cm at the site. Over the Ferris Coal seam is a siltstone that has
606 irregular structures that could potentially be signs of paleosol and is 22 cm thick. The following
607 facies is a layer of shale for 14 cm, with silty siltstone overlying the shale for 36 cm, with the top
608 most 5 cm having coarser grain sizes. Superimposed over the siltstone is silty claystone and is
609 about 130 cm thick, with this facies being overlain by a silty mudstone that was 125 cm thick.
610 The next facies up was a thin ironstone cap that was 15 cm thick with an iron-rich mudstone over
611 the cap that was 140 cm in thickness, with the level of iron being more concentrated at the base
612 compared to the top. A siltstone overlies the mudstone for 170 cm, with a thin organic rich
613 siltstone for 10 cm, with the final facies being a mudstone paleosol with possible root traces that
614 was 75 cm thick before going into glacial till.
615

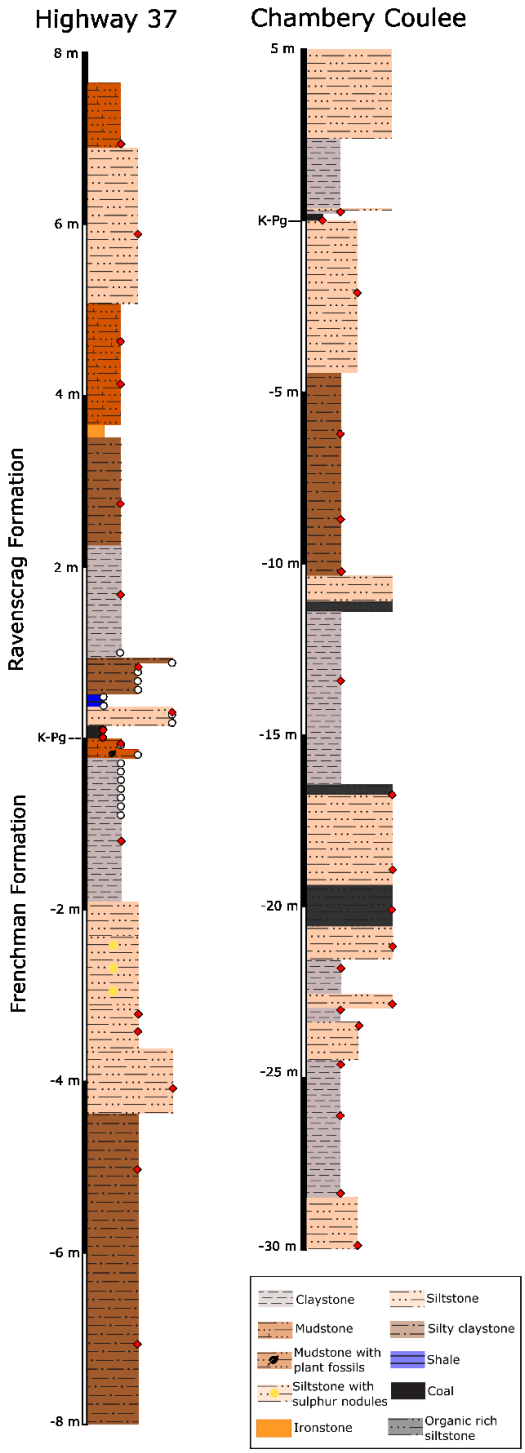

Figure 7: Stratigraphic sections for Highway 37 and Chambery Coulee with corresponding legend. The white circles in the Highway 37 section marks where samples were collected during 2018, while the red diamonds mark where samples were collected during 2017.

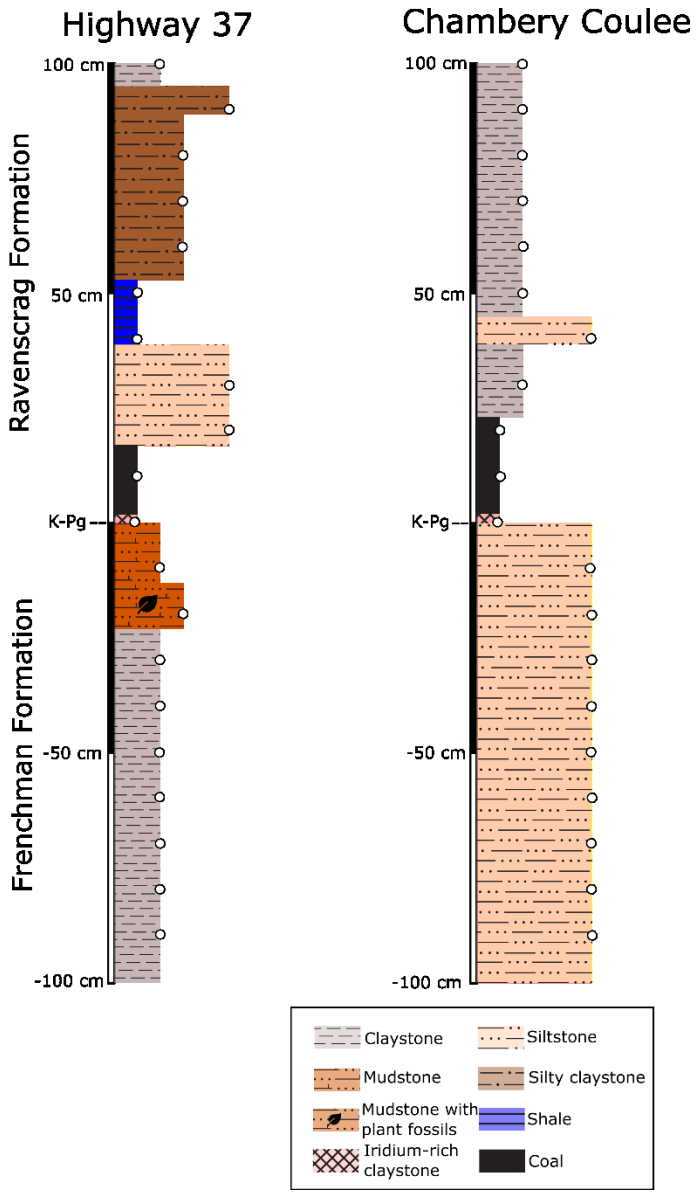

620

621 Figure 8: Stratigraphic sections for the 2-meter sampling interval from the 2018 expedition for Highway 37 and

622 Chambery Coulee with corresponding legend. The white circles mark where the corresponding samples were

623 collected during 2018.

624

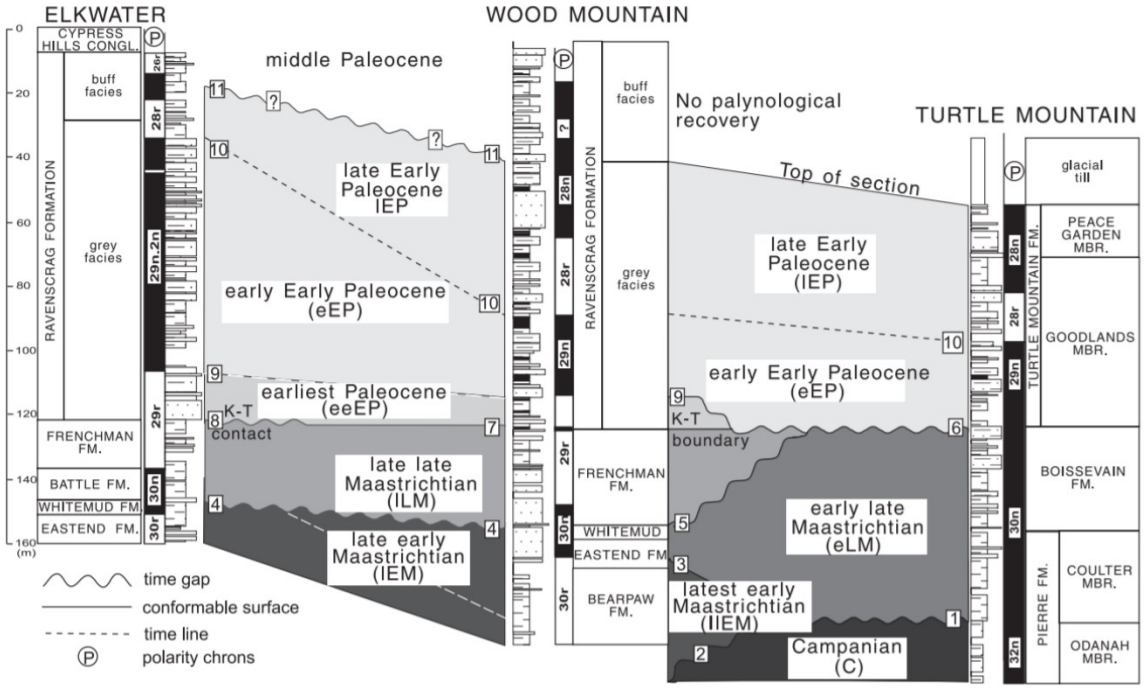

Figure 9: Several stratigraphic sections of sites from southern Canada, with Wood Mountain being the closest to our sample sites as it is also from southern Saskatchewan. (Catuneanu & Sweet, 1999)

2.2.3 Sample collection

Sampling in 2017 focused on collection of a preliminary set of samples from each section at relatively low resolution with one sample being taken from distinct sedimentary units at each of the sites. Sampling in 2018 focused on high-resolution sampling within a 1 m window above and below the K-Pg boundary. Two types of samples were collected for different sets of analyses, with larger samples with an average weight of 300 mg collected for the primary leaf wax analysis whereas smaller samples of only 5 mg were collected for bulk organic carbon and $\delta^{13}C$ analyses at 2 cm intervals over a 2 m range across the K-Pg boundary. In total, 159 large samples were collected across both sites; 19 samples were collected from Chambery Coulee during the first field season and 40 during the second field season while 17 samples were collected from Highway 37 during the first field season and 38 during the second field season,

though of these only 22 samples from Chambery Coulee and 25 samples from Highway 37 were analyzed due to time constraints, and these were samples focused in the 2 meter span around the boundary.

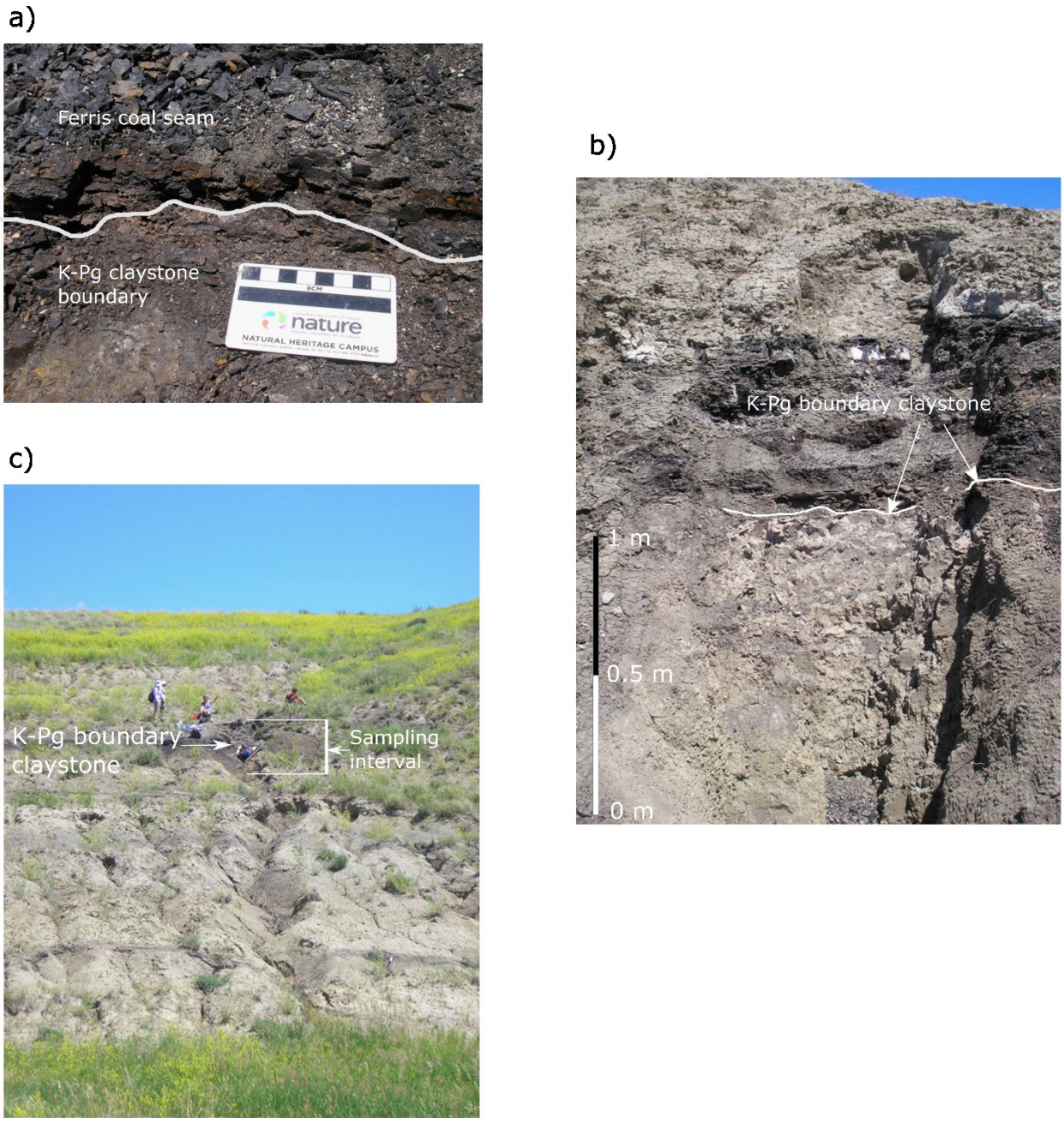

Figure 10: Photos from the field work of 2018. Close up of the K-Pg boundary from Chambery Coulee, a faintly pink-brown layer of clay found underneath the dark shelf of coal above, with the scale bar level with the boundary

(a). 2-meter Chambery Coulee section exposed in frame, the dark layer centered in the image is the Ferris coal seam with the boundary sandwiched between the coal layer and the larger bed of siltstone below it (b). Field site by the roadside of Highway 37 (c), with the two meter section focused on for this study around where my field assistants Aidan Olivier Howenstine, Claudia Selles, and Tony Smith are seated, along with local paleontologist Emily Bamforth and her field assistant Hallie Street.

2.3 Methodology

2.3.1 Organic carbon and bulk $\delta^{13}C$ analyses

Samples were prepared in the lab for the initial analysis with around 5 mg of material being prepared per sample. Each sample was then ground to a fine powder with a mortar and pestle. The samples of organic carbon content and bulk $\delta^{13}C$ ($\delta^{13}C_{bulk}$) values were analyzed from the sediment samples at the University of Quebec at Montreal. The samples were acid fumigated in silver capsules prior to analysis to remove inorganic carbon (Harris et al., 2001). The silver capsules were then closed and placed within tin capsules to be analyzed, with the samples being processed on an Isoprime 100 MicroCube mass spectrometer coupled to an Elemental Vario MicroCube elemental analyzer in Continuous Flow mode to either measure the organic carbon weight against the total weight of carbon within each sample or analyze the $\delta^{13}C_{bulk}$ value.

2.3.2 Lipid extraction and analysis

Sediment was prepared for the lipid extraction process by weight and ground into a fine powder with any roots particles removed. The amount of sediment extracted varied depending on organic carbon content (measurements described above), with carbon-rich samples typically

requiring 40 g of sediment while carbon-poor samples required up to 200 g of sediment to yield sufficient n-alkanes for isotopic analysis. The sediments for the 2017 batches and the Highway 37 2018 batch were prepared by being put into CEM MARS solvent extraction tubes with a 200 ul of stock solution consisting 2 mg of n-Docosane D-46, Pentadecanoic acid D-29, n-Octadecyl D-37 Alcohol, and 4 ml of hexane. A 9:1 ratio of dichloromethane (DCM) to methanol solution was then prepared for each sample, with the volume of solvent scaled to the volume of sediment. Samples were then microwaved in a MARS6 microwave in the lab at a temperature of 80° C for 15 minutes, which extracts organic molecules from the sediments into the DCM-methanol mixture when heated. The last batch of samples for Chambery Coulee 2018 did not have stock solution added as the stock solution was used for identifying the location of the peaks and was no longer necessary for this batch of samples as the timing of the peaks was found to be consistent between different batches of samples. Samples were then transferred into vials to be centrifuged, separating sediment from solvent, before pippeting the solvent and transferring it to separate vials for evaporation. The sediment was then further rinsed with solvent and centrifuged three times. Once all the samples were prepared, they were placed within a Rapidvap, a device that heats up and evaporates samples under N_2 gas, for concentrating the molecules for the next step. A silica gel column was then prepared for lipid purification, with a Pasteur pipette filled with 1 g of silica gel on top of glass wool, and 0.5 g of sodium sulphate. Each vial had 15 ml of hexane added and was passed through their own silica gel column to elute the fraction and collect it. We then collected the polar fraction by eluting 15 ml of methanol, followed by 1 ml of dichloromethane. The polar fraction was reserved for future study.

The samples were then analyzed for *n*-alkane concentration using a thermo Trace 13-10 gas chromatograph (GC) with a flame ionization detector (-FID). We quantified the X, Y, Z, etc

694 *n*-alkanes. *n*-Alkane hydrogen and carbon isotope measurements were made using a Thermo
695 Delta V Plus Isotope Ratio Mass Spectrometer (IRMS) coupled to a Thermo GC-IsoLink. The
696 first run was for carbon, both to verify with the results from the GC-FID and to measure the
697 amount required for sufficient readings, though this is followed by a run for the hydrogen
698 isotopes. The samples are prepared for the hydrogen run in separate vials as less material is
699 needed but at a higher concentration. A 300 µl vial is inserted into a larger 500 µl vial with a
700 support underneath to keep the smaller vial stable. The original sample is then evaporated down
701 to a smaller volume, roughly 100 µl or so, just enough to fit in the 300 µl vial easily and is then
702 fully evaporated. Once all the samples are evaporated, a specified amount of hexane is added to
703 each sample to provide the ideal peak heights, this is also based on how much of the sample will
704 be taken up during injection. Isotope measurements on the IRMS are reported using delta
705 notation, measuring the isotopic ratios of carbon relative to the abundance of carbon-13 while the
706 isotopic ratios of hydrogen were relative to the abundance of hydrogen-2 (deuterium). The
707 equation for the delta notation of hydrogen is as follows:

708 $$\delta^2 H = \left(\frac{{}^2R_H - {}^2R_{std}}{{}^2R_{std}}\right) * 1000 \quad \textbf{1.}$$

709 The equation for the delta notation of carbon is as follows:

710 $$\delta^{13} C = \left(\frac{{}^{13}R_C - {}^{13}R_{std}}{{}^{13}R_{std}}\right) * 1000 \quad \textbf{2.}$$

711 The above equations express the isotopic ratios relative to the Vienna Standard Mean
712 Ocean Water (V-SMOW) for hydrogen and Vienna Pee Dee Belemnite (V-PDB) for carbon,
713 with the standards in the lab calibrated using n-alkane standards from Indiana University
714 (arndt.schimmelmann.us/compounds.ht). Internal standards were also prepared for the purpose of
715 standardizing field samples and ensure the instruments were in functioning order. The internal
716 standards used the hydrogen and carbon isotope values of native *Acer sp.* leaves that were

717 collected on McGill campus, with synthetic alkanes added to enhance the C_{22} and C_{30} peaks.
718 Standards run after every 3 samples to correct for instrumental drift. The overall standard
719 deviations (STDEV) used to justify accurate $\delta^{13}C$ measurements were around 0.5‰, while the
720 STDEV used for $\delta^{2}H$ measurements were around 5‰. The total average of the standard
721 deviations across the days where samples used in the analyses were analyzed were 0.26‰ for
722 $\delta^{13}C$ and 4.03‰ for $\delta^{2}H$.
723
724 *2.3.3 Relative chain length abundance analyses*
725 We also calculated to indices of the relative abundance of different chain lengths within
726 each sample as they provide additional information along with the isotopic measurements. The
727 average chain length (ACL) calculates the average chain length based on the area underneath the
728 curves of peaks that represent each chain length (Fig. 11 for example), which is multiplied by the
729 corresponding number of carbon molecules in the given lipid chain. These are then added
730 together and divided by the sum of the areas in the previous measurement, with the formula
731 layout given below.
732 $$ACL = \frac{(A23*23)+(A24*24)+(A25*25)+(A26*26)+(A27*27)+(A28*28)+(A29*29)+(A30*30)+(A31*31)}{A23+A24+A25+A26+A27+A28+A29+A30+A31} \quad \textbf{3.}$$
733 This value can be used to see whether short or long chain alkanes are more abundant,
734 which in of itself can be related to whether the plant waxes are primarily being derived from
735 aquatic or terrestrial plants, as longer chain alkanes are typically produced from terrestrial plants
736 while aquatic plants tend to produce more shorter chain alkanes (Ficken et al., 2000).
737 An additional calculation to be made with this data is the Paq' (Liu et al., 2019), a similar
738 calculation that is used to judge if plant waxes are primarily derived from aquatic or terrestrial
739 plants. Similarly, to the ACL, the Paq' uses the areas derived from the peaks in the abundance of

individual lipid chains in samples, though this time only focusing on the odd numbered chains that are produced by plants. This specific calculation is intended to be used in the context of ancient, sediment-derived plant waxes rather than from living ecosystems. The calculation is as follows.

$$Paq' = \frac{A21+A23+A25}{A21+A23+A25+A27+A29+A31+A33} \quad \textbf{4.}$$

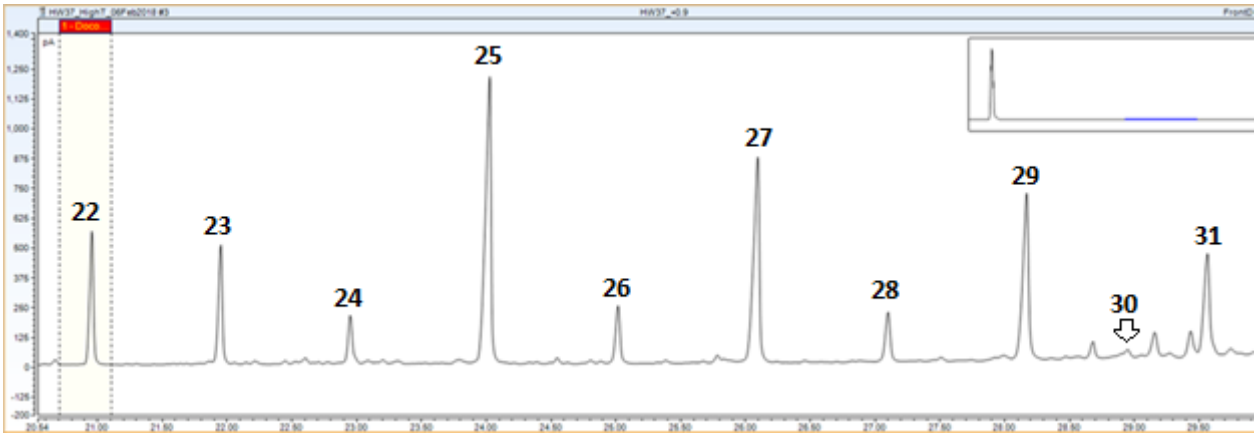

Figure 11: GC-FID results from sample HW +0.9, from the 2017 field season, with the lipid chains C_{27}, C_{29}, and C_{31} peaks highlighted. This is an example of relative lipid peak abundances.

2.4 Results

2.4.1 Percent organic carbon

The first batch of results took the midpoint of each distinct stratigraphic unit to measure the organic content present at each of the two sites (Fig. 12 b, Fig. 13 b). A total of 17 samples from Highway 37 (Table 1) and 19 samples from Chambery Coulee (Table 2) were taken during 2017 for the percent organic carbon analysis. None of the strata in the Frenchman Formation

758 below the boundary had an organic content higher than 1%, with the lowest values reaching less
759 than 0.01% at both Highway 37 (Fig. 12 b) and Chambery Coulee (Fig. 13 b). The values at the
760 boundary range from 2.08% at Chambery Coulee to 43.01% at Highway 37. The coal layer
761 found above the boundary at both sites have organic content of 34.20% at Highway 37 to 47.89%
762 at Chambery Coulee. Measurements above the boundary differ between the sites, with Chambery
763 Coulee only having the coal layer sampled above the boundary, while Highway 37 dropping in
764 value from 0.12% to 14.79% organic carbon.

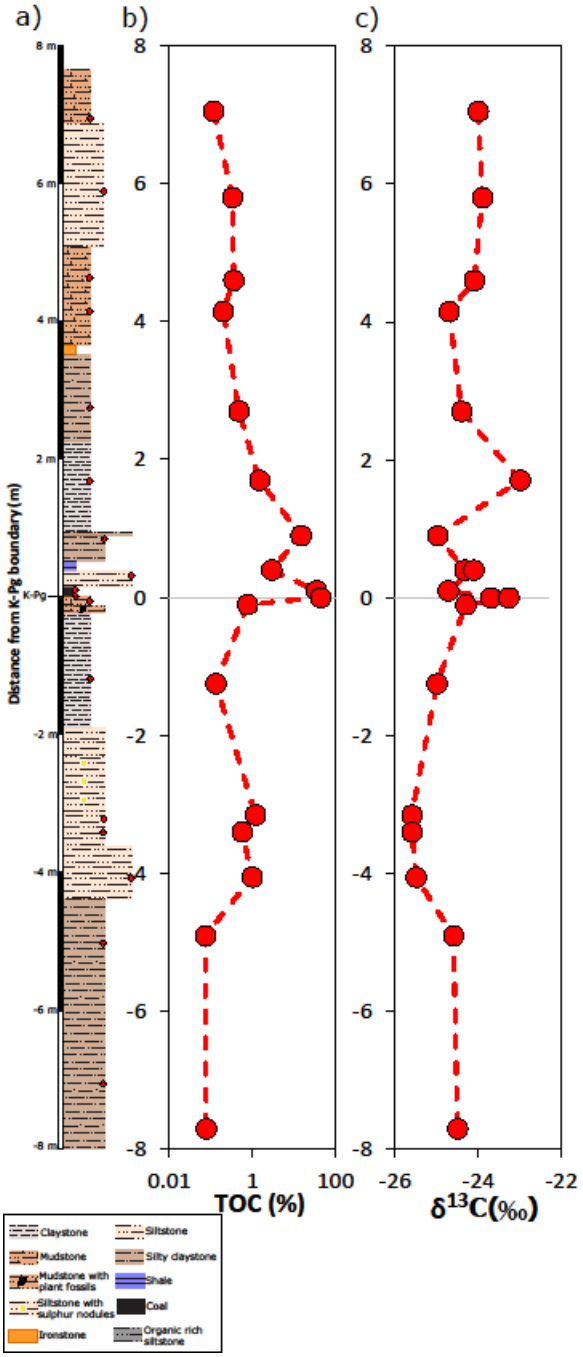

765

766 Figure 12: Measurements of total organic carbon and $\delta^{13}C_{bulk}$ made from the 2017 Highway 37 section. TOC values

767 plotted on a logarithmic scale in order to highlight variability below the boundary.

768

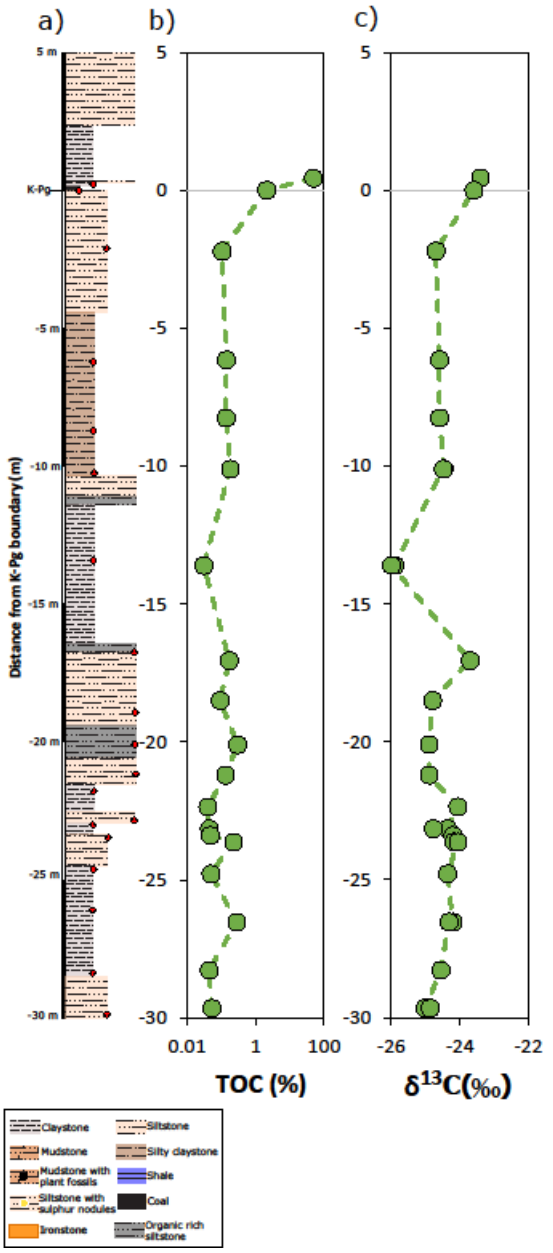

769

770 Figure 13: Measurements of total organic carbon and $\delta^{13}C_{bulk}$ made from the 2017 Chambery Coulee section. TOC

771 values plotted on a logarithmic scale in order to highlight variability below the boundary.

772

773 The second batch of results focused on a two-meter interval around the K-Pg boundary at

774 Chambery Coulee and Highway 37 with the results of the data having been taken 2 cm intervals

775 within the 20 cm around the boundary and at 4 cm intervals beyond those points (Fig. 14 b, Fig.

15 b). In total, 69 samples from Highway 37 and 68 samples from Chambery Coulee were measured for the percent organic carbon values in 2018 (Table 3). Below the boundary at Chambery Coulee (Fig. 15 b), there is a steady rise in organic carbon percentage up to the boundary from 0.28% to 0.91% while the samples at Highway 37 (Fig. 14 b) also show a general rising trend up to the boundary, though with more fluctuations and a greater range of values, with the most depleted value of 0.04% at 68 cm below the boundary while the most enriched sample had 8.15% organic carbon at 28 cm below the boundary. At the boundary, Highway 37 had a higher value at 10.07% whereas Chambery Coulee had a lower value at 2.60%. Above the boundary, both sites had values ranging from 28.47% to 70.07% at the carbon rich coal layers immediately above the boundary, which are then followed by drops in the range of 0.40% to 1.12% before rising back up, with the two signals no longer overlapping with distance from the boundary. After reaching a peak of 12.48% at Highway 37 and 24.33% at Chambery Coulee, the values upward in the sequence decrease in value, with Chambery Coulee experiencing a much sharper and severe drop in organic content than Highway 37.

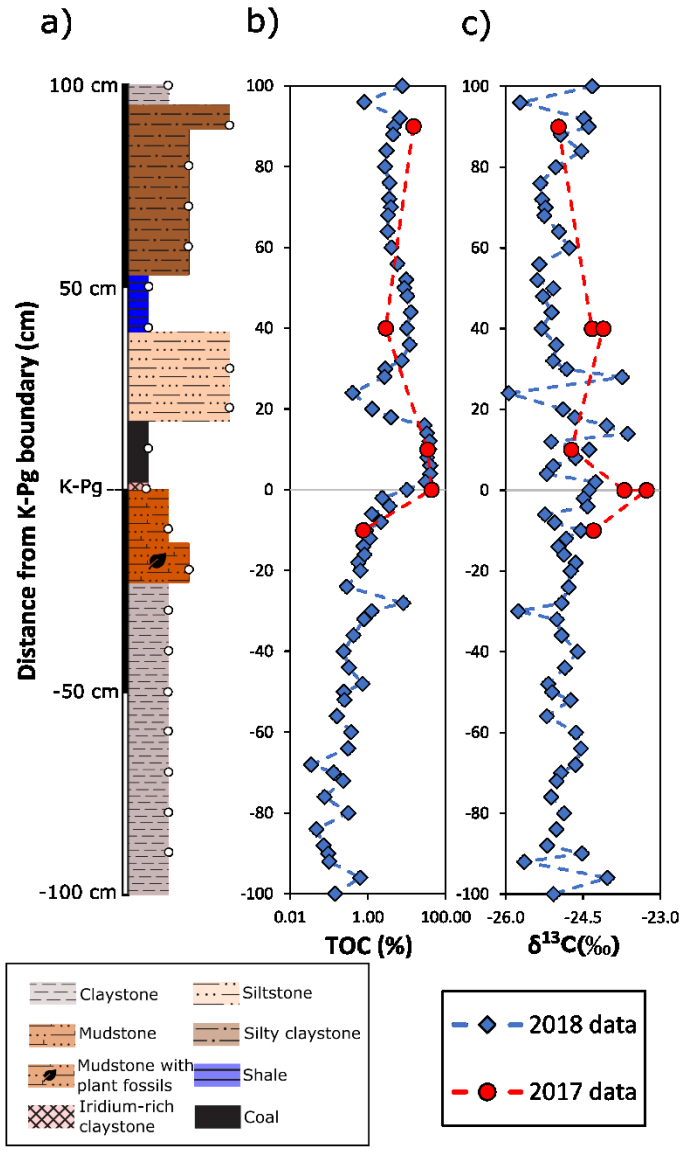

791

792 Figure 14: Measurements of total organic carbon and $\delta^{13}C_{bulk}$ made from the 2018 Highway 37 section with 2017

793 data for comparison. TOC values plotted on a logarithmic scale in order to highlight variability below the boundary.

794

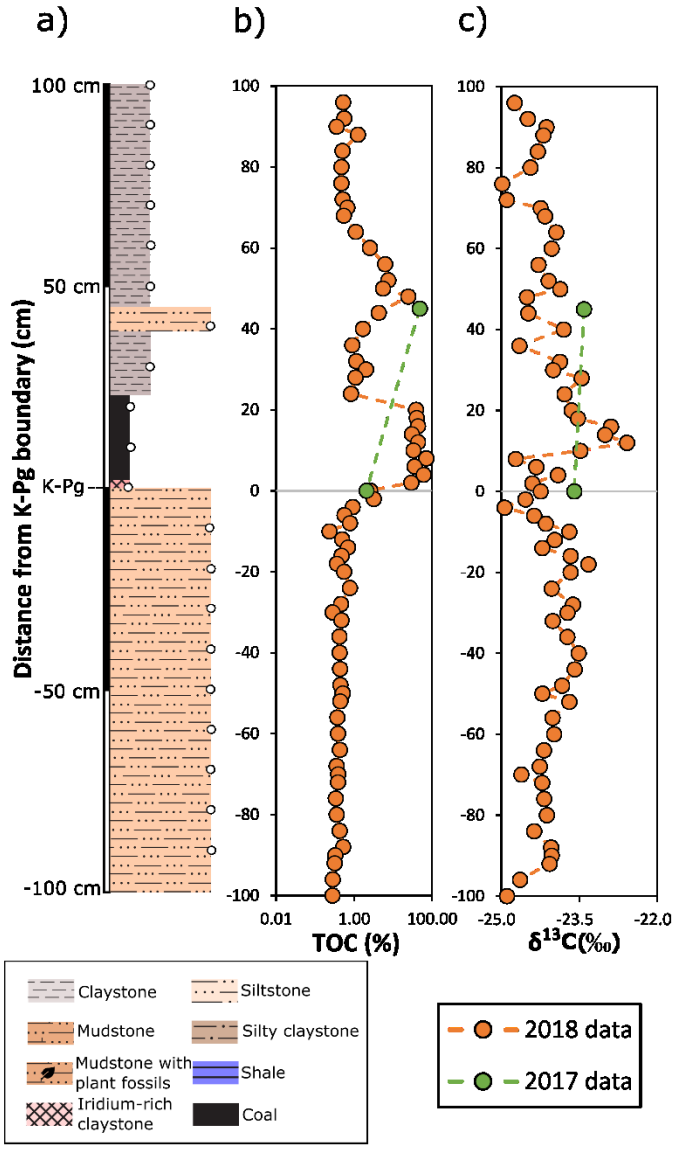

Figure 15: Measurements of total organic carbon and $\delta^{13}C_{bulk}$ made from the 2018 Chambery Coulee section with 2017 data for comparison. TOC values plotted on a logarithmic scale in order to highlight variability below the boundary.

2.4.2 Bulk organic carbon $\delta^{13}C$

The results of the 2017 study show a mixture of $\delta^{13}C_{bulk}$ signals across the different sites (Fig. 12 c, Fig. 13 c). As the bulk organic carbon measurements used the same samples as the total organic carbon measurements with only a few duplicates analyzed, meaning 19 samples

804 from Highway 37 (Table 1) and 25 samples from Chambery Coulee analyzed for these results
805 (Table 2). At Highway 37 (Fig. 12 c) there is a drop from -24.60‰ to -25.60‰ from 4.9 meters
806 below the boundary to 3.4 meters below the boundary, shifting from siltstone to more organic-
807 rich mudstones before $\delta^{13}C_{bulk}$ rises back up to 24.30‰ immediately below the boundary.
808 Chambery Coulee (Fig. 13 c) shows a high degree of fluctuations between -24.06‰ and -26.0‰
809 across a variety of facies across almost 20 meters before remaining relatively stable at -24.60‰
810 for the 10 meters leading up to the boundary. Highway 37 and Chambery Coulee share very
811 similar values for the $\delta^{13}C_{bulk}$ at the boundary with the values of -23.70‰ and -23.60‰
812 respectively. Above the boundary presents a rather peculiar scenario, as the coal layers do not
813 show a highly negative value that would line up with the negative carbon isotope excursion
814 presented at other boundaries, though this is almost certainly just a by-product of the low
815 resolution between samples, as previous studies have shown that the negative carbon isotope
816 excursion occurs in the first 3 to 5 cm above the boundary (Arens and Jahren, 2000; Maruoka et
817 al., 2007; Therrien, 2007; Yamamoto et al., 2010). As the focus of this initial sample collection
818 was to collect a single sample from each distinct facies, it made it likely that the negative carbon
819 isotope excursion would be missed due to the purposely low sample resolution. Upward from the
820 boundary, the values at Highway 37 fluctuate between facies with no consistent pattern beyond
821 an overall increasing trend in $\delta^{13}C_{bulk}$ with a minimum value of -24.85‰ to a maximum of -
822 23.00‰, and Chambery Coulee's one sample collected above the boundary only has a slightly
823 more positive value than the boundary at -23.41‰.
824 The results of the data collected from the summer of 2018 provide a more in-depth look
825 due to the more high-resolution nature at a closer two-meter interval around the K-Pg boundary
826 (Fig. 14 c, Fig. 15 c). As with the 2017 data, the 2018 $\delta^{13}C_{bulk}$ measurements used the same

827 samples as the percent organic carbon, with 69 samples from Highway 37 and 68 samples from
828 Chambery Coulee having been measured (Table 3). The samples from Highway 37 (Fig. 14 c)
829 remain relatively stable with only some fluctuation below the boundary between -24.03‰ and -
830 25.76‰, while at Chambery Coulee (Fig. 15 c) there is a slight rise in $\delta^{13}C_{bulk}$ from -24.89‰ to -
831 23.52‰ over 60 cm before it slowly begins to decline up to the boundary, reaching as low as -
832 24.94‰. The values at the boundary are very similar at both sites, with Highway 37 having a
833 value of -24.38‰ and Chambery Coulee having a value of -24.25‰. The samples above the
834 boundary show a high degree of variation with little correlation between the two sites, with large
835 shifts in values occurring over small intervals. Additionally, even at 2 cm resolution near the
836 boundary there is no clear trace of the negative isotope excursion, which is odd as Jerrett et al.,
837 2015, which had taken measurements in the Frenchman River Valley where the sites of
838 Chambery Coulee and Highway 37 are located, displayed a negative isotope excursion of -
839 26.21‰ within the first 4 cm of the boundary, yet the two sites show a relatively stable signal
840 over that interval. Beyond the first 30 cm of the boundary, the signals at the two sites begin to
841 stabilize, still with some variation between samples, but never greater than about 0.8‰, a similar
842 range to what was observed before the impact.
843
844 *2.4.3 Average chain length*
845 The ACL (equation 3) was calculated for the 2018 samples from Highway 37 (Fig. 16 d)
846 and Chambery Coulee (Fig. 17 d) around the boundary at both sites, with the ACLs of just the
847 odd chains displayed and the numbers on the x-axis corresponding to the number of carbon
848 molecules in a given chain. The ACL measurements for both sites were taken for samples that
849 had signals that were clear and distinct enough to be read, with Highway 37 having 20

850 measurements and Chambery Coulee having 17 measurements (Table 8). For Highway 37, the
851 ACL The ACL at Highway 37 remained relatively stable with average length between 26.5 and
852 27.5, with even odd and even chain lengths remaining within that range. By contrast, Chambery
853 Coulee showed a much greater range below the boundary from around 25.3 to 26.3. Both sites
854 also show very similar values for the K-Pg boundary with ACL of just under 26.5. Above the
855 boundary, both sites show a large increase in the ACL, with Highway 37 reaching an ACL of
856 28.5 at 20 cm above the boundary while Chambery Coulee reached an ACL of 27.9 at 10 cm
857 above the boundary. This peak is then followed by a reduction in the ACLs at both sites before
858 values rise again, sharply at Highway 37 and more gradually at Chambery Coulee. The samples
859 from above the boundary at Highway 37, starting from around 50 cm above the boundary,
860 stabilize to values similar to those before the impact at around 27, while at Chambery Coulee
861 they are longer above the boundary, with ACLs between 26.0 and 27.4.

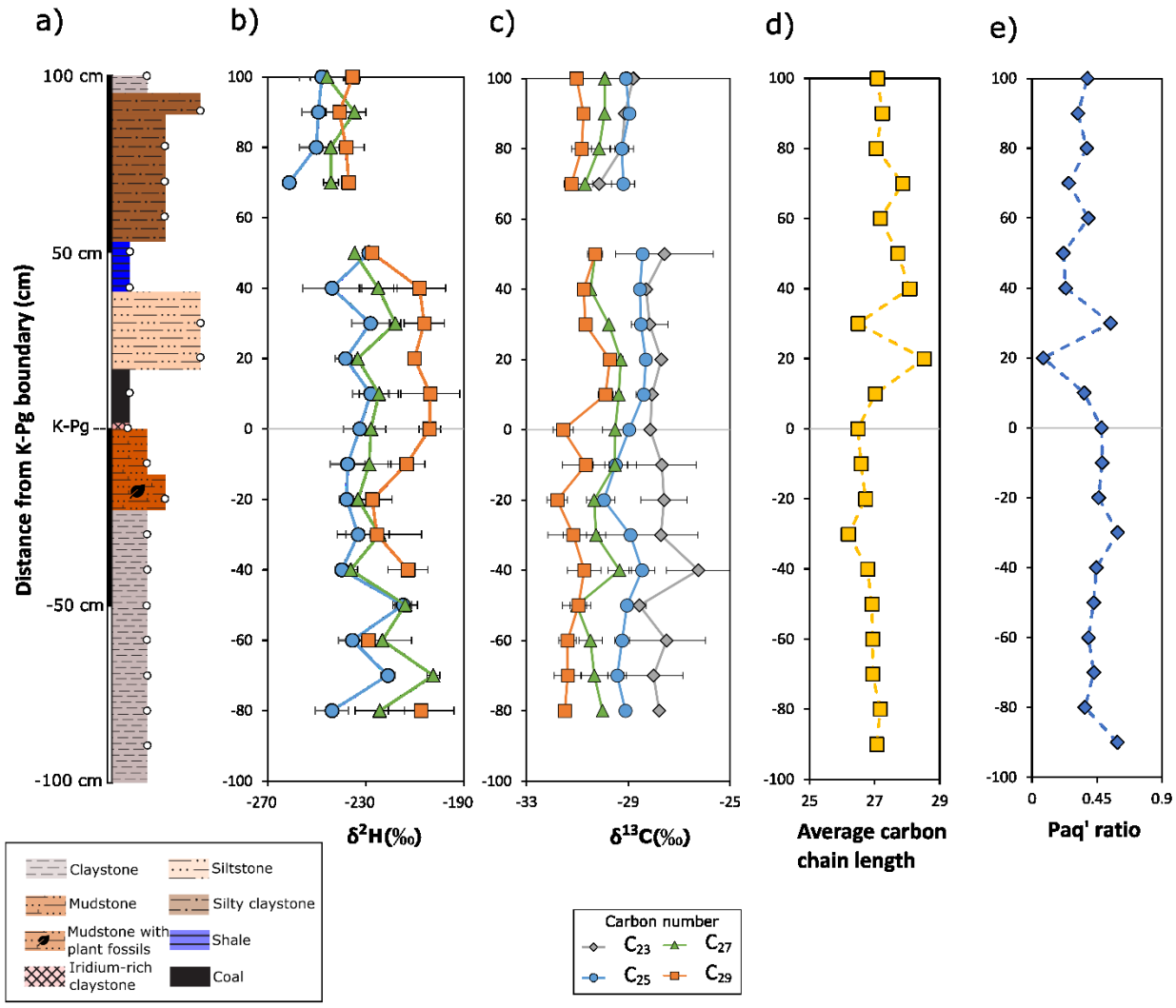

862

863 Figure 16: The measurements and calculations made from the Highway 37 section in relation to plant wax isotopes.

864 Pictured are the stratigraphic section (a), the δ^2H (b) and $\delta^{13}C$ (c) stable isotope measurements derived from plant

865 wax lipids, the average chain length measurements (d) and the Paq' calculations made from the relative abundance

866 of different plant wax lipid chains to estimate the abundance of plant waxes from aquatic vs terrestrial plants (e).

867

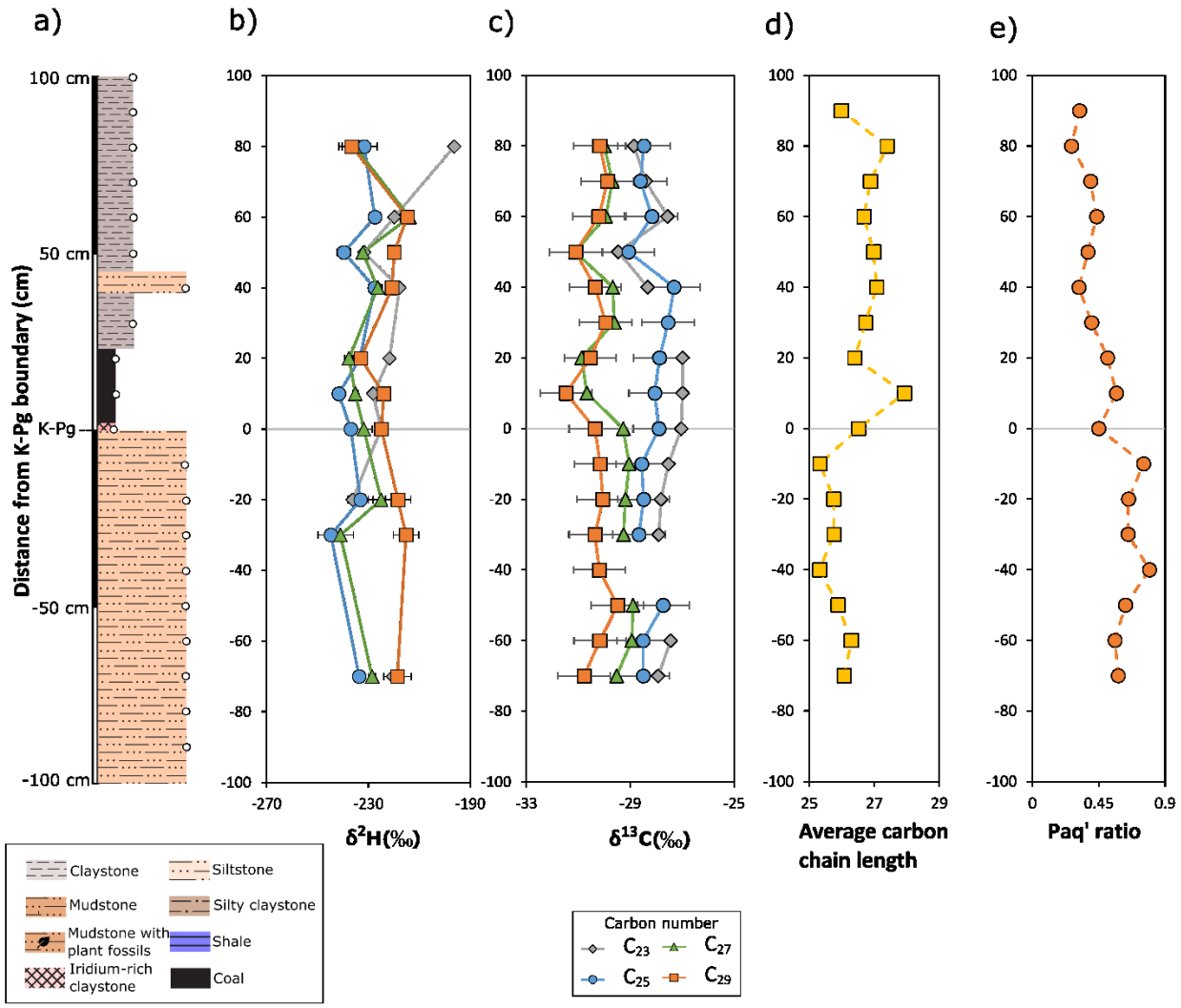

Figure 17: The measurements and calculations made from the Chambery Coulee section in relation to plant wax isotopes. Pictured are the stratigraphic section (a), the δ^2H (b) and $\delta^{13}C$ (c) stable isotope measurements derived from plant wax lipids, the average chain length measurements (d) and the Paq' calculations made from the relative abundance of different plant wax lipid chains to estimate the abundance of plant waxes from aquatic vs terrestrial plants (e).

2.4.4 Paq'

The relative abundance of individual lipid chain lengths were taken from the GC-FID and used in the calculation of the Paq' (Liu et al., 2019) to judge if plant waxes are primarily derived

878 from aquatic or terrestrial plants. As the Paq' uses the same concentration measurements as
879 ACL, there were also 20 results from Highway 37 and 17 results from Chambery Coulee (Table
880 8). The calculation in question (equation 4) is as follows. Measurements for all lipid chains were
881 used with the exception of C_{33}, as the signal for those lipids was too minor to reasonably extract
882 from the majority of the data sets. However, it is reasonable to assume that this would not have
883 significantly influenced the data, as the C_{31} areas were very low relative to the other peaks. The
884 C_{31} areas from Chambery Coulee and below the boundary at Highway 37 have a range of areas
885 from 0.0516 to 43.1942, with these values consistently being the smallest values in the Paq'
886 measurements. Paq' values (Fig. 16 e, Fig. 17 e) from Highway 37 (Fig. 16 e) are generally
887 lower than those collected from Chambery Coulee (Fig. 17 e), while the Paq' values at Highway
888 37 that are greater than contemporary Chambery Coulee samples are only greater by as much as
889 0.1. Highway 37 values below the boundary stay within a range from 0.4 to 0.6 while at
890 Chambery Coulee they stay at a range from 0.6 to 0.8 over the same interval. Both sites have
891 fairly consistent results at the boundary with Highway 36 having a Paq' of 0.5 at the boundary
892 while Chambery Coulee has 0.5. A major shift occurs above the boundary at both sites, with
893 samples almost consistently lower above the boundary than below it. The Highway 37 values
894 generally range from 0.2 to 0.4 with an extreme low value of 0.1 at 20 cm above the boundary
895 and an extreme high value of 0.5 at 30 cm above the boundary. Chambery Coulee has more
896 consistent values ranging from 0.3 to 0.6 with a continuous decrease in values over the first 40
897 cm above the boundary, followed by a rise and fall over the next 40 cm.
898
899 *2.4.5 Hydrogen plant wax isotope measurements*

The isotope values of carbon and hydrogen were obtained from plant wax lipids of different length based on the number of carbon molecules in each lipid chain, with chain lengths of 23, 25, 27, and 29 carbon molecules focused on for this study. For Highway 37, there were 19 samples measured for C_{25} and C_{27} chain lengths and 17 samples measured for C_{29} (Table 6), while Chambery Coulee had 9 samples measured for C_{23} and 10 samples measured for C_{25}, C_{27}, and C_{29} chain lengths (Table 7). At Highway 37 (Fig. 17 b), the δ^2H values for each chain length were within the range of -203‰ to -261‰, with C_{25} on average having the most negative values at -236‰ and C_{29} having the highest values with an average of -219‰, with C_{27} having values between the other two lipid chain lengths with an average of -228‰. The Chambery Coulee (Fig. 17 b) samples range from -196‰ to -245‰, also showing C_{29} to typically have the most positive values with an average of -223‰ and C_{25} tending to have the most negative with an average of -235‰. However, C_{23} fluctuates relative to the other chain lengths but has an average value of -222‰, with C_{27} also maintaining values between those of C_{25} and C_{29} with an average of -231‰. Points that are missing values did not have sufficiently high concentration to provide reliable measurements.

2.4.6 Carbon plant wax isotope measurements

For the carbon plant wax isotope measurements, Highway 37 had 18 samples measured for C_{23}, C_{25}, C_{27}, and C_{29} chain lengths (Table 4) while Chambery Coulee had 13 samples measured for C_{23}, 15 for C_{25} and C_{27}, and 16 for C_{29} chain lengths (Table 5). The $\delta^{13}C$ values obtained from Highway 37 (Fig. 17 c) range from -26.2‰ to -31.8‰, with the shorter hydrocarbon chains consistently having more positive values than those of longer chain lengths, with C_{23} measurements averaging at -28.1‰ while C_{29} averaged at -30.9‰. This extends to the

other two hydrocarbon chains measured, with C_{25} having an average value of -29.0‰ and C_{27} having an average of -30.0‰. Each hydrocarbon length has values that stay within 2‰ with all the chain lengths showing distinct trends through the section (Fig. 18). The Chambery Coulee (Fig. 17 c) samples range from -27.0‰ to -31.5‰, maintaining the same pattern as Highway 37 with the shorter chain length hydrocarbons having more positive values. This is shown in the average values for each lipid chain length, with the C_{23} values averaging at -27.9‰, C_{25} values averaging at -28.2‰, C_{27} values averaging at -29.7‰, and C_{29} values averaging at -30.3‰. The range of values for individual chains is relatively similar, with the largest range being about 2.5‰ for C_{23}. Due to the more incomplete nature of this sample set, the periodic pattern is less extensive in this sample set than it is in the Highway 37 data, although the peaks and valleys of individual periods are still distinct at several points within the graphs (Fig. 16 c, Fig. 17 c).

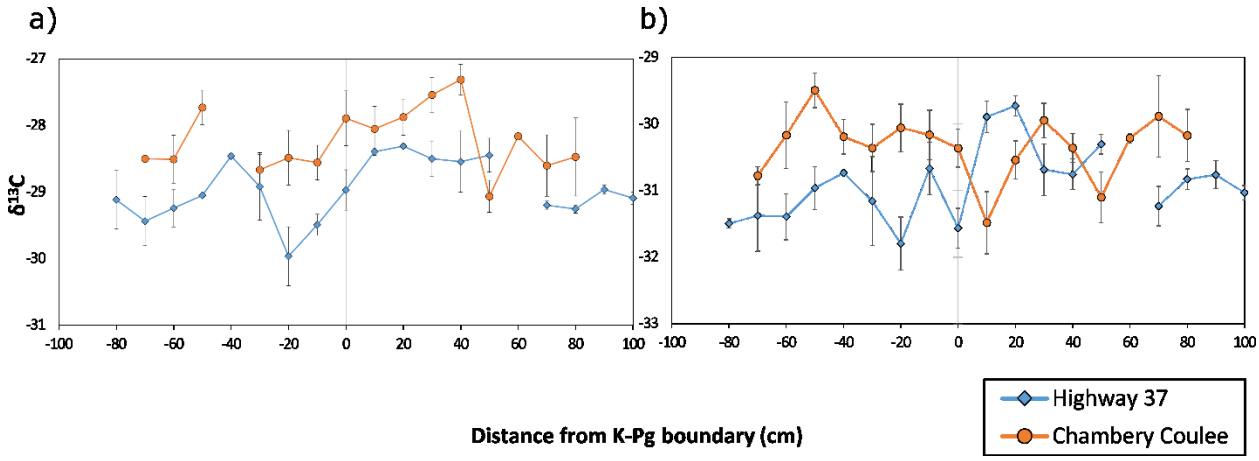

Figure 18: $\delta^{13}C$ measurements of C_{25} (a) and C_{29} (b) being compared between the two sites to better display similarities and differences in the overall trends observed through the stratigraphic sections.

2.5 Discussion

941 *2.5.1 Isotopic differences between plant wax chain lengths*

942 *2.5.1.1 Carbon isotopes*

943 n-Alkane carbon isotope measurements from both sites show periodic variability where
944 $\delta^{13}C$ values rise and fall over periodic intervals through the sample sections, which is most clear
945 for the C_{25} and C_{29} lipid chains. The Highway 37 section (Fig. 16 c) shows the chains for C_{25} and
946 C_{29} behaving in a similar manner through the section, with $\delta^{13}C$ rising and falling in the same
947 stratigraphic units, the only exception being directly at the boundary where the C_{29} value dips
948 down, which may represent the short-term K-Pg carbon isotope excursion identified at other
949 terrestrial sections. The general interpretation of plant wax lipids from sediments is that C_{25} is
950 primarily derived from aquatic plants while C_{29} is inferred to primarily be derived from
951 terrestrial plants and are thus influenced by different factors to produce the carbon isotopic
952 compositions that are observed (Ficken et al., 2000; Aichner et al., 2010). Aquatic plants have
953 more enriched isotopic compositions due to isotopic exchange in water. As water has a higher
954 viscosity than air, particles in the water move much more slowly and it makes it more difficult
955 for plants to selectively utilize the lighter carbon that is otherwise energetically preferred, thus
956 resulting in higher concentrations of $\delta^{13}C$ (Keeley & Sandquist, 1992). The data extracted is
957 consistent with Keeley & Sandquist (1992)'s observation with the C_{25} carbon isotopes being
958 more enriched in carbon-13 across all the samples, showing that this is an interpretation that is
959 valid for the dataset. The significance of the two chains behaving in a similar manner suggests
960 that the forces controlling carbon isotope fractionation had a similar affect on both aquatic and
961 terrestrial systems at Highway 37. By contrast, the Chambery Coulee section (Fig. 17 c) shows
962 two different patterns between C_{25} and C_{29}. Chambery Coulee's C_{25} signal resembles the
963 trajectory observed at Highway 37, with the samples becoming more enriched across the

boundary. The C_{29} values fluctuate more frequently, with enrichment peaks about twice as frequent as the Highway 37. This suggests that while aquatic plants at the site experienced similar forcing as the plants at Highway 37, the difference in C_{29} and C_{25} at Chambery Coulee suggests that some other factors were over-printing the more regional effects for terrestrial plant life at this locale. In addition, the C_{29} value 10 cm above the boundary shows a distinct drop in $\delta^{13}C$, which suggests this could represent part of the carbon isotope excursion for this site.

2.5.1.2 Hydrogen isotopes

The n-alkane hydrogen isotopes show little to no trend across the study interval of both sites, with individual chain lengths not following similar temporal patterns when comparing between the two sites. This lack of a pattern is also accompanied by a narrow range of values for the isotopic composition, suggesting that little over all change occurred in the isotopic composition at the sites. The only possible exception to this is a long-term decline of 20 to 30‰ that is evident in the C_{27} and C_{29} data at both sites (Fig. 16 b, Fig. 17 b), though the rate of decline can not be determined as an accurate rate of sedimentation can not be determined. This observation suggests that little change had occurred in the regional hydrological cycle over the depositional period that was examined, with the minor changes that are observed likely being local in nature, given the lack of consistency between the two sites. Furthermore, the complete lack of any major shifts after the boundary suggest that, if the impact did have an affect on the isotopic composition of precipitation, it was short lived to have recovered within the time deposition of merely 10 cm, and did not cause a major change in the hydrological cycle that persisted over a long period of time. This also rules out the possibility of prolonged droughts as there is no indication of increased evaporation rates over the sampling interval that was examined.

In addition to the raw values extracted from the plant waxes, the values of the δ^2H of precipitation were calculated in order to properly compare our data with modern values in order to reconstruct the hydrological system of the area. An assumption had to be made for the fractionation of hydrogen isotopes in lipid biosynthesis, and for our analysis we assumed a fractionation value of -100‰, as this is considered the average of C3 fractionation within conifers and angiosperms (Sachse et al., 2012), the dominant woody trees across the Cretaceous-Paleogene boundary globally (Saward, 1992; Sweet et al., 1999). The most notable observation for the δ^2H of precipitation is the low values of the samples, with all the chain lengths averaging between -100 and -180‰, values that are quite low to be found in rain water. These values are in fact surprisingly similar to the δ^2H values from precipitated water in present day western Canada (values taken from wateriso.utah.edu, Bowen, 2019; Bowen & Revenaugh, 2003; IAEA/WMO, 2015). Due to how both sites share this trait it would make sense that this is a regional feature and makes sense given the geography of the region, as the localities are within the rain shadow of the still developing Rockies. While the rain shadow effect was probably the main contributing factor to the depleted δ^2H values, other effects may have also contributed to the measurements observed in the plant wax record. The other contributing factor would include the higher latitude at the time of deposition at during the end of the Cretaceous (Spicer & Herman, 2010), determined to be around 15° further north in the late Campanian (this value would be lower by the end of the Maastrichtian though no exact measurements have been made for this time period), which would also have lowered the δ^2H values as a result of how hydrogen isotopes in plant waxes are affected by temperature (Sachse et al., 2012). One interesting comparison is that similarly depleted values have been recorded in slightly older sediments from the Late Santonian to Late Campanian sediments of the Canadian Arctic (Super et al., 2018), though it is highly

unlikely the isotopic composition of precipitation from both sites were depleted from the same mechanisms. Another interesting point of the depleted δ^2H values is that the Western interior seaway, was in relatively close proximity to the sites, which suggests that the rain water from the region was coming from the Pacific Ocean on the other side of the mountains in spite of the seaway being so close. However, the apparent long-term trend of decreasing values over time may in fact coincide with the retreat of the western interior seaway that began during the latest Maastrichtian, possibly explaining the negative trend. If this is the case though, more work is needed to know over what time frame this negative trend was occurring and how significant it was, as this data set does not cover the entire time span, with the current minimum of the possible shift being 20-30‰ with no upper limit yet defined.

2.5.2 Relative lipid chain abundance

Paq' with a value above 0.4 is interpreted that waxes were derived primarily from aquatic plants while a Paq' of below 0.4 is interpreted as primarily coming from terrestrial plants (Liu et al., 2019). Below the boundary at Chambery Coulee, Paq' values are consistently above the 0.4 threshold while at Highway 37 most of the samples are above 0.4 with a few at lower values. This suggests the plant waxes from Chambery Coulee were primarily derived from aquatic plants while at Highway 37 it was a likely mix of aquatic and terrestrial plant input. Across the boundary for both sites there is a shift from aquatic to terrestrial plant values, with the shift occurring below the boundary at Highway 37. Above the boundary the Highway 37 values are consistently below 0.4 throughout the section with the exception of 30 cm above the boundary while at Chambery Coulee the samples are very close to 0.4, suggesting that at Highway 37

terrestrial plants primarily contributed to the samples while there was a mixture of terrestrial and aquatic plant waxes being contributed to Chambery Coulee.

This observation was then compared with the ACL measurements as well as the observed trends of the C_{27} lipid chains. The ACL measurements strongly match the Paq' trend with the Chambery Coulee samples (Fig. 17 d). While C_{29} chains are primarily produced by terrestrial plants, C_{27} lipids are produced by both aquatic and terrestrial plants, providing an alternative means of interpreting the input of lipids from terrestrial and aquatic plants. This is done by looking at how close the C_{27} values are to those of C_{25} and C_{29} as the aquatic plants have higher $\delta^{13}C$ values while the terrestrial plants have more negative per mil values (Fig. 16 c, Fig. 17 c). What is interesting is that at both sites C_{27} behaves similarly across the boundary, with values below the boundary more often being much closer to C_{25}, which more strongly reflect aquatic plants, though this does not necessarily mean they were more abundant. Across the boundary there is a notable shift at both Highway 37 and Chambery Coulee where C_{27} values shift from higher values closer to those of C_{25} towards lower values closer to C_{29} over a 20 cm span. While there is some variability, the increase in the ACL that occurs after the boundary followed by the gradual drop over time is comparable to the results of another study looking at plant wax lipids across the K-Pg boundary (Yamamoto et al., 2010). While it is interesting that the more limited source of the leaf waxes still show a shift to longer chained lipids after the boundary, it is more than likely that the similar signals recorded at both sites are merely coincidental, as northern Africa and western Canada were vastly different ecosystems and at different latitudes, making the similar shift an intriguing possibility rather than a definitive trend in plant system recovery.

Between the different observations there is a strong case to be made that a shift in the source of plant wax lipids in the depositional environments of both sites are observed across the

data sets, with a primarily aquatic origin observed before the boundary and in the earliest sediments above the boundary at Chambery Coulee, while Highway 37 shows a mixed signal of aquatic and terrestrial plant input. Above the boundary, Highway 37 shows a signal that is more strongly the result of terrestrial plant input while Chambery Coulee fluctuates, with primarily aquatic plant input immediately after the boundary before transitioning into terrestrial plant input and then returning to aquatic plant input and then once more returning to more terrestrial influenced input. This suggests that a major shift occurred at or after the boundary that affected the flora of the entire local sedimentary basin. This is especially odd as the strata immediately above the boundary is a coal layer, and for the shift in hydrogen isotopes to indicate a change to more terrestrial plant life seems almost counterintuitive. One possibility is that the environments in which these coals formed were swamps with open water, primarily composed of standing vegetation rather than aquatic plants. Another possibility would be an ecological shift in the plant life occurring as a result of the extinction event with a shift to more terrestrial plants being present in the ecosystem, however this can not be verified without more fossils or pollen spores.

2.5.3 Bulk organic carbon isotope data

It is notable that the $\delta^{13}C_{bulk}$ record from both Highway 37 and Chambery Coulee do not exhibit the negative carbon isotope excursion that appears above the boundary in other K-Pg boundary, where other studies have noted it in the first 3-5 cm (Jerrett et al., 2015; Maruoka et al., 2007; Therrien, 2007; Yamamoto et al., 2010). While at Highway 37 there is a negative excursion 24 cm above the boundary, the excursion itself is quite small at -1.56‰ (Fig. 14 c). Notably the excursion is found in nearby sites, where it reaches values as low as -2‰ and at 2 to 3 cm above the boundary (Jerrett et al., 2015) and that other excursions of similar value can be

found above the boundary (Therrien et al., 2007). This is in contrast with our own data, where the values at the boundary show a rise in $\delta^{13}C_{bulk}$ at both sites compared to values from before the boundary. Although unusual, the variable and ambiguous degree of the excursion has been observed elsewhere (Maruoka et al., 2007; Therrien, 2007; Yamamoto et al., 2010), where it has been shown that across different sites the location and degree of the negative isotope excursion is variable relative to the boundary claystone. It is also important to note that the preservation of the excursion could have affected its position. This is primarily controlled by the rate of deposition, though erosion or lack of proper depositional conditions could have led to the complete lack of the excursion appearing in the data. This argument does not hold up well as the lack of any signs of sedimentary unconformities and the preservation of the boundary claystone along with the Ferris coal seams present above the boundary claystone do not support the likelihood of the negative excursion having been eroded out of the sequence.

Along with the lack of a distinct negative carbon isotope excursion, both sites show a high degree of amplitude variability at the 10 to 30 cm interval above the boundary. Despite the lack of an obvious signal for the negative isotope excursion, the presence of this kind of signal indicates some kind of environmental disturbance. This type of variation in the $\delta^{13}C_{bulk}$ cannot have been caused by changes in the carbon isotope composition of plant primary productivity as it would have been observed in the plant wax derived isotope data. One possible explanation for the variation includes increased productivity from benthic plants, which would also lead to the rapid increases in $\delta^{13}C_{bulk}$ due to the naturally higher values they have relative to terrestrial plants (Keeley & Sandquist, 1992). However, this interpretation is inconsistent with the observations from ACL (Fig. 16 c, Fig. 17 c) or Paq' (Fig. 16 d, Fig. 17 d), as those measurements indicate a larger input from terrestrial plants rather than from aquatic plants. An alternative explanation

implicates microbial respiration. Enhanced aerobic respiration in soils could lead to more positive values to be recorded in sedimentary organic matter (Natelhoffer & Fry, 1988), and so occasional increases in microbial respiration could lead to rapid increases in the $\delta^{13}C_{bulk}$ record followed by drops to more typical levels. Additionally, the more negative values that appear at both sites over this interval would be the result of microbial respiration in an anaerobic environment which would result in the fractionation of more negative values. This may suggest that depositional/general soil conditions switched between anaerobic and aerobic over several intervals for some time after the Chicxulub impact yet well after plant communities had recovered (Lomax et al., 2001; Maruoka et al., 2007). One possible explanation for alternating anaerobic and aerobic environments would be related to boom and bust cycles in plant communities with large build ups of plant diversity followed by collapses resulting in decreased diversity. These collapses could potentially be the result of unstable systems from communities recovering after the extinction event without systems having reached a steadier equilibrium, with the anaerobic conditions arising from higher rates of decomposition from oxygen consuming bacteria. The more aerobic conditions would reflect a healthy plant community that would account for the more positive values we see associated with aerobic respiration. The only issue with this idea is that the conditions for anaerobic and aerobic microbial growth are also controlled by hydrological conditions, and as the hydrogen values from both sites do not show any patterns or signs that reflect what is observed in the bulk carbon data, this still remains unresolved. Palynological data would be needed to further investigate this suggestion, though it is not unwarranted as it would be occurring after plant communities have largely recovered from the extinction event or that some other, non botanical factors are driving these changes.

2.5.4. Geochronology and the timing of environmental change

The chronology of the records of environmental change contained in our studied sediments is not well constrained. However, we can make generalized estimates of the timespan of the sections based on the negative carbon isotope excursion at the boundary inferred from the C_{29} carbon *n*-alkane measurements (Fig. 14 c, Fig. 15 c). At Chambery Coulee we observed the negative carbon at around 20 cm above the boundary and around 10 cm above the boundary at Highway 37. Using radiometric age constraints for the duration of the CIE from the Hell Creek Formation (Renne et al., 2013), which was measured to be 5,000 ± 3,000 years after the iridium-rich boundary, we can then estimate that these sites deposited at a deposited one cm every 250-500 years. Using this estimate, the upward trend in *n*-alkane $\delta^{13}C$ values spanning the K-Pg boundary observed at both sites was approximately 20,000 to 25,000 years in duration. This would be consistent with precession forced carbon cycle variability, although given the uncertain stratigraphy of the CIE in these sediments this interpretation is speculative. The mechanisms for such large magnitude (~2‰) precession-driven $\delta^{13}C$ variability is unclear, especially given the absence of a clear signal of hydrological change in the $\delta^{2}H$ data.

2.5.5 Relation to the K-Pg extinction

One of the most distinct features about this study is that no lasting changes are observed in the plant wax record above the K-Pg boundary (Fig. 16 b, Fig. 16c, Fig. 17 b, Fig. 17 c). None of the lipid chains for hydrogen and carbon at both sites show a massive shift occurring at the boundary, with the only exception being C_{29} at Highway 37 (Fig. 16 c) which becomes more negative, suggesting that the changes experienced for these cycles were not instantaneous. Furthermore, the carbon cycles show that there were no long lasting disturbances to the cycles

after the impact as there is no apparent disruption to the cyclical patterns between the boundary and the next sample 10 cm above it. This suggests that if the carbon cycles were affected that they had not only recovered in a relatively short amount of time, but also that the extinction event did not disrupt the Milankovitch cyclicity in the carbon cycles. Furthermore, the hydrogen isotope data further supports this with no large offsets in values after the boundary, with samples remaining rather stable. This suggests that both the terrestrial carbon and hydrological cycles had recovered in a relatively quick period of geologic time of probably no more than 10 thousand years. This is consistent with other studies that have suggested similar or even lower durations for the recovery time of terrestrial environments (Fastovsky et al., 2016; Lomax et al., 2001; Maruoka et al., 2007; Renne et al., 2013). Additionally, the large carbon isotope variability observed is not consistent with volcanic inputs of atmospheric CO_2. Volcanic CO_2 input would be very similar isotopically to background atmospheric CO_2 (Mason et al., 2017), implying that very large amounts of CO_2 would needed to produce the 2‰ variability observed in the plant waxes. As a result of the data available, no strong case can be made for or against the activity of the Deccan traps, at least in regards to them having an effect on the carbon and water cycles.

2.6 Conclusions

The isotopic study of plant wax lipids across the K-Pg boundary has revealed a number of details from the region previously unknown or that have not been explored. Precipitation in the region appears to be primarily derived from the Pacific Ocean due to highly depleted δ^2H with a further decrease over time being linked to the retreat of the Western Interior Seaway. $\delta^{13}C$ measurements show signs of fluctuation that are on comparable time scales to the precession

orbital cycles, suggesting climatological effects related to these isotopic shifts was affecting local plant life. The lack of an obvious disturbance to the hydrogen or carbon isotope measurements across the boundary suggests both the water and carbon cycles recovered within 16,000 years after the impact. However after the impact there is a notable shift in the dominant plant species contributing to the collection of plant waxes, suggesting that plant communities experienced a dynamic shift that lasted for some time after the extinction event. Additionally, a high degree of disturbance in the bulk carbon record after the impact suggests a period of instability which is here interpreted as being related to conditions shifting between those favouring anaerobic or aerobic respiring bacteria.

2.7 Acknowledgements

The authors would like to thank Emily Bamforth for her assistance and guidance in the field of the summers of 2017 and 2018. Thanks to Agnieszka Adamowiscz-Walczak and Jean-Francois Helie for their aid with analyses at the Geotop Stable Isotope Lab at UQAM. We thank Thi Hao Bui for managing the lab and aiding with setting up and running the GC and mass spectrometer that were integral to this study. I also would like to thank the Allemand family for allowing me to collect material on their land. This research was funded thanks to NSERC funding to Peter Douglas, as well as Anita Mountjoy, the Redpath Museum, and the Earth and Planetary Science Department which provided funding to Robert Bourque.

Tables

Table 1: Bulk $\delta^{13}C$ and organic carbon percentage from Highway 37, 2017.

Distance from boundary (cm)	HW37 2017 - $\delta^{13}C_{bulk}$	STDEV – HW37 2017 - $\delta^{13}C_{bulk}$	HW37 2017 - Corg
705	-24.00	0.30	0.12
580	-23.90	0.30	0.33
460	-24.10	0.30	0.35
415	-24.70	0.30	0.20
270	-24.40	0.30	0.47
170	-23.00	0.30	1.47
90	-24.98	0.30	14.79
40	-24.33	0.30	2.87
40 - duplicate	-24.11	0.30	
10	-24.73	0.30	34.20
0	-23.70	0.30	43.01
0 - duplicate	-23.27	0.30	
-10	-24.30	0.30	0.76
-125	-25.00	0.30	0.13
-315	-25.60	0.30	1.17
-340	-25.60	0.30	0.56
-405	-25.50	0.30	1.00
-490	-24.60	0.30	0.07
-770	-24.50	0.30	0.08

1191

1192 **Table 2:** Bulk $\delta^{13}C$ and organic carbon percentage from Chambery Coulee 2017.

Distance from boundary (cm)	CC 2017 - $\delta^{13}C_{bulk}$	STDEV – CC 2017 - $\delta^{13}C_{bulk}$	CC 2017 - Corg
45	-23.41	0.30	47.89
0	-23.60	0.30	2.08
-220	-24.70	0.30	0.10
-615	-24.60	0.30	0.14
-825	-24.60	0.30	0.14
-1010	-24.47	0.30	0.18
-1010 - duplicate	-24.49	0.30	
-1360	-25.91	0.30	0.03
-1360 - duplicate	-26.00	0.30	
-1705	-23.70	0.30	0.17
-1850	-24.80	0.30	0.09
-2010	-24.90	0.30	0.30
-2120	-24.90	0.30	0.13
-2235	-24.07	0.30	0.04
-2315	-24.37	0.30	0.04
-2315 - duplicate	-24.78	0.30	
-2339	-24.21	0.30	0.05
-2363	-24.18	0.30	0.23
-2363 - duplicate	-24.06	0.30	

-2478	-24.36	0.30	0.05
-2653	-24.21	0.30	0.28
-2653 - duplicate	-24.33	0.30	
-2828	-24.56	0.30	0.04
-2966	-25.02	0.30	0.05
-2966 - duplicate	-24.87	0.30	

Table 3: Bulk $\delta^{13}C$ and organic carbon percentage, 2018.

Distance from boundary (cm)	HW37 - $\delta^{13}C_{bulk}$	STDEV - HW37 - $\delta^{13}C_{bulk}$	HW37 - Corg	CC - $\delta^{13}C_{bulk}$	STDEV - CC - $\delta^{13}C_{bulk}$	CC - Corg
100	-24.32	0.30	7.69			
96	-25.72	0.30	0.81	-24.75	0.30	0.52
92	-24.48	0.30	6.62	-24.49	0.30	0.56
90	-24.39	0.30	4.69	-24.13	0.30	0.36
88	-24.94	0.30	4.46	-24.19	0.30	1.24
84	-24.53	0.30	3.04	-24.30	0.30	0.50
80	-25.03	0.30	2.76	-24.44	0.30	0.47
76	-25.33	0.30	3.56	-24.98	0.30	0.47
72	-25.29	0.30	3.52	-24.90	0.30	0.51
70	-25.23	0.30	3.93	-24.25	0.30	0.67
68	-25.25	0.30	3.32	-24.16	0.30	0.54

64	-24.97	0.30	3.24	-23.94	0.30	1.09
60	-24.77	0.30	4.07	-24.03	0.30	2.50
56	-25.35	0.30	5.71	-24.29	0.30	6.15
52	-25.39	0.30	9.55	-24.09	0.30	7.47
50	-25.08	0.30	8.70	-23.87	0.30	5.53
48	-25.28	0.30	10.35	-24.51	0.30	24.33
44	-25.11	0.30	12.48	-24.48	0.30	4.24
40	-25.30	0.30	10.13	-23.80	0.30	1.68
36	-25.02	0.30	11.76	-24.66	0.30	0.89
32	-25.08	0.30	7.45	-23.87	0.30	1.12
30	-24.82	0.30	2.82	-24.00	0.30	1.99
28	-23.74	0.30	2.68	-23.46	0.30	1.09
24	-25.94	0.30	0.40	-23.79	0.30	0.83
20	-24.89	0.30	1.31	-23.65	0.30	38.32
18	-24.66	0.30	3.91	-23.53	0.30	40.00
16	-24.04	0.30	28.47	-22.89	0.30	43.01
14	-23.64	0.30	32.64	-23.01	0.30	30.08
12	-25.12	0.30	38.20	-22.58	0.30	43.18
10	-24.38	0.30	37.63	-23.48	0.30	32.84
8	-24.65	0.30	33.80	-24.73	0.30	70.07
6	-25.08	0.30	39.68	-24.33	0.30	35.25
4	-25.20	0.30	39.78	-23.91	0.30	60.35
2	-24.26	0.30	30.19	-24.40	0.30	29.14

0	-24.38	0.30	10.07	-24.25	0.30	2.60
-2	-24.49	0.30	2.33	-24.54	0.30	3.16
-4	-24.41	0.30	3.58	-24.94	0.30	0.91
-6	-25.24	0.30	1.26	-24.37	0.30	0.56
-8	-25.05	0.30	2.17	-24.15	0.30	0.78
-10	-24.55	0.30	0.90	-23.70	0.30	0.23
-12	-24.83	0.30	1.13	-23.97	0.30	0.49
-14	-24.98	0.30	0.77	-24.21	0.30	0.69
-16	-24.87	0.30	0.82	-23.67	0.30	0.47
-18	-24.65	0.30	0.57	-23.33	0.30	0.36
-20	-24.74	0.30	0.65	-23.67	0.30	0.55
-24	-24.78	0.30	0.29	-24.03	0.30	0.78
-28	-24.91	0.30	8.15	-23.62	0.30	0.46
-30	-25.76	0.30	1.25	-23.73	0.30	0.28
-32	-25.01	0.30	0.80	-24.01	0.30	0.47
-36	-24.92	0.30	0.42	-23.73	0.30	0.42
-40	-24.60	0.30	0.24	-23.52	0.30	0.42
-44	-24.85	0.30	0.33	-23.59	0.30	0.44
-48	-25.18	0.30	0.73	-23.83	0.30	0.44
-50	-25.10	0.30	0.24	-24.21	0.30	0.51
-52	-24.75	0.30	0.25	-23.70	0.30	0.44
-56	-25.20	0.30	0.16	-24.02	0.30	0.37
-60	-24.64	0.30	0.37	-23.99	0.30	0.38

-64	-24.54	0.30	0.31	-24.18	0.30	0.43
-68	-24.65	0.30	0.04	-24.26	0.30	0.36
-70	-24.93	0.30	0.13	-24.62	0.30	0.39
-72	-25.01	0.30	0.23	-24.22	0.30	0.38
-76	-25.12	0.30	0.08	-24.18	0.30	0.34
-80	-24.87	0.30	0.31	-24.12	0.30	0.35
-84	-25.02	0.30	0.05	-24.37	0.30	0.43
-88	-25.20	0.30	0.07	-24.04	0.30	0.52
-90	-24.52	0.30	0.10	-24.03	0.30	0.33
-92	-25.64	0.30	0.10	-24.08	0.30	0.32
-96	-24.03	0.30	0.64	-24.64	0.30	0.28
-100	-25.08	0.30	0.14	-24.89	0.30	0.28

1195

1196 **Table 4:** Highway 37 $\delta^{13}C$ measurements from plant wax lipids.

Distance from boundary (cm)	HW37 - C_{23} $\delta^{13}C$ (‰)	STDEV - HW37 - C_{23} $\delta^{13}C$ (‰)	HW37 - C_{25} $\delta^{13}C$ (‰)	STDEV - HW37 - C_{25} $\delta^{13}C$ (‰)	HW37 - C_{27} $\delta^{13}C$ (‰)	STDEV - HW37 - C_{27} $\delta^{13}C$ (‰)	HW37 - C_{29} $\delta^{13}C$ (‰)	STDEV - HW37 - C_{29} $\delta^{13}C$ (‰)
100	-28.8	0.1	-29.1	0.1	-29.9	0.1	-31.0	0.1
90	-29.1	0.7	-29.0	0.1	-29.9	0.0	-30.8	0.2
80	-29.3	0.2	-29.3	0.1	-30.2	0.1	-30.8	0.2
70	-30.1	1.9	-29.2	0.1	-30.7	0.0	-31.2	0.3
50	-27.6	0.3	-28.4	0.3	-30.3	0.1	-30.3	0.1
40	-28.3	1.4	-28.5	0.5	-30.5	0.3	-30.8	0.2
30	-28.2	0.5	-28.5	0.3	-29.8	0.5	-30.7	0.4
20	-27.7	0.1	-28.3	0.0	-29.3	0.0	-29.7	0.2
10	-28.1	0.2	-28.4	0.1	-29.4	0.1	-29.9	0.2
0	-28.1	0.1	-29.0	0.3	-29.5	0.1	-31.6	0.3
-10	-27.7	0.1	-29.5	0.2	-29.5	0.5	-30.7	0.4
-20	-27.6	0.9	-30.0	0.4	-30.3	0.3	-31.8	0.4

-30	-27.7	1.3	-28.9	0.5	-30.3	0.5	-31.2	0.7
-40	-26.2	NA	-28.5	0.0	-29.3	0.2	-30.7	0.0
-50	-28.6	NA	-29.1	0.0	-31.0	0.6	-31.0	0.3
-60	-27.5	1.5	-29.2	0.3	-30.5	0.5	-31.4	0.3
-70	-28.0	1.2	-29.4	0.4	-30.3	0.5	-31.4	0.5
-80	-27.8	1.3	-29.1	0.4	-30.0	0.8	-31.5	0.9

Table 5: Chambery Coulee δ13C measurements from plant wax lipids.

Distance from boundary (cm)	CC - C_{25} $\delta^{13}C$ (‰)	STDEV - CC - C_{25} $\delta^{13}C$ (‰)	CC - C_{27} $\delta^{13}C$ (‰)	STDEV - CC - C_{27} $\delta^{13}C$ (‰)	CC - C_{29} $\delta^{13}C$ (‰)	STDEV - CC - C_{29} $\delta^{13}C$ (‰)
80	-28.5	0.6	-30.0	0.2	-30.2	0.4
70	-28.6	0.5	-29.7	0.6	-29.9	0.6
60	-28.2	0.0	-29.9	0.2	-30.2	0.1
50	-29.1	0.2	-31.1	0.4	-31.1	0.4
40	-27.3	0.2	-29.7	0.2	-30.4	0.2
30	-27.5	NA	-29.6	NA	-29.9	NA
20	-27.9	0.3	-30.9	0.3	-30.5	0.3
10	-28.1	0.3	-30.7	0.2	-31.5	0.5
0	-27.9	0.4	-29.3	0.3	-30.4	0.3
-10	-28.6	NA	-29.0	NA	-30.2	0.4
-20	-28.5	0.4	-29.2	0.4	-30.1	0.4
-30	-28.7	0.2	-29.3	0.2	-30.4	0.4
-40					-30.2	NA
-50	-27.7	NA	-28.9	NA	-29.5	NA
-60	-28.5	0.4	-28.9	0.6	-30.2	0.5
-70	-28.5	0.0	-29.5	0.3	-30.8	0.1

Table 6: Highway 37 δ^2H measurements from plant wax lipids.

Distance from boundary (cm)	HW37 - C_{25} δ^2H (‰)	STDEV - HW37 - C_{25} δ^2H (‰)	HW37 - C_{27} δ^2H (‰)	STDEV - HW37 - C_{27} δ^2H (‰)	HW37 - C_{29} δ^2H (‰)	STDEV - HW37 - C_{29} δ^2H (‰)
100	-248	9	-246	7	-235	3
90	-249	7	-235	5	-241	6
80	-250	7	-244	3	-238	7
70	-261	2	-244	3	-237	2
50	-229	1	-235	1	-228	0
40	-244	12	-225	8	-208	11
30	-228	8	-218	2	-206	8

20	-238	4	-233	1	-210	2
10	-228	7	-225	8	-204	12
0	-233	6	-228	6	-204	4
-10	-237	7	-229	9	-213	8
-20	-238	3	-233	7	-227	8
-30	-233	5	-224	17	-226	NA
-40	-240	3	-236	3	-213	8
-50	-215	3	-214	NA		
-60	-236	5	-223	12	-229	NA
-70	-221	3	-203	3		
-80	-244	7	-224	10	-208	13
-90	-207	1	-206	1	-188	26

1201

1202 **Table 7:** Chambery Coulee δ^2H measurements from plant wax lipids.

Distance from boundary (cm)	CC - C_{23} δ^2H (‰)	STDEV - CC - C_{23} δ^2H (‰)	CC - C_{25} δ^2H (‰)	STDEV - CC - C_{25} δ^2H (‰)	CC - C_{27} δ^2H (‰)	STDEV - CC - C_{27} δ^2H (‰)	CC - C_{29} δ^2H (‰)	STDEV - CC - C_{29} δ^2H (‰)
80	-196	NA	-232	NA	-235	NA	-237	NA
60	-220	NA	-227	1	-214	0	-215	1
50	-232	NA	-240	3	-232	1	-220	2
40	-218	NA	-227	2	-226	2	-221	2
20	-222	NA	-233	1	-238	2	-233	2
10	-228	NA	-242	2	-235	1	-224	3
0	-225	NA	-237	2	-232	3	-225	2
-20	-236	NA	-233	NA	-225	NA	-218	NA
-30			-245	NA	-241	NA	-215	NA
-70	-220	NA	-234	0	-229	1	-219	5

1203

1204 **Table 8:** Paq' and average chain length measurements.

Distance from boundary (cm)	HW37 - Paq'	CC - Paq'	HW37 - ACL	HW37 - ACL (odd only)	CC - ACL	CC- ACL (odd only)
100	0.4		27.1	27.2		
90	0.3	0.3	27.2	27.3	26.0	27.4
80	0.4	0.3	27.0	27.1	27.4	27.5
70	0.3	0.4	27.9	27.9	26.9	27.0
60	0.4	0.4	27.2	27.3	26.7	26.7
50	0.2	0.4	27.7	27.8	27.0	27.0

40	0.2	0.3	28.1	28.3	27.1	27.1
30	0.5	0.4	26.5	26.4	26.7	26.8
20	0.1	0.5	28.5	28.6	26.4	26.4
10	0.4	0.6	27.0	27.0	27.9	28.1
0	0.5	0.4	26.5	26.5	26.5	26.5
-10	0.5	0.8	26.6	26.6	25.3	25.3
-20	0.5	0.7	26.7	26.6	25.8	25.7
-30	0.6	0.6	26.2	26.2	25.8	25.7
-40	0.4	0.8	26.8	26.8	25.3	25.3
-50	0.4	0.6	26.9	27.0	25.9	25.8
-60	0.4	0.6	26.9	27.1	26.3	26.3
-70	0.4	0.6	26.9	27.1	26.1	26.0
-80	0.4		27.2	27.2		
-90	0.6		27.1	27.1		

1205

1206

Chapter 3: Primary conclusions and future directions

The most significant conclusions to be taken from this study are the following.

1. The lack of a clear negative excursion from either site lends credence to the idea that the negative carbon isotope excursion should not be relied on as a definitive marker for the K-Pg boundary due to unreliable depositional requirements.
2. The bulk $\delta^{13}C$ values from the sediments show a high degree of variance above the K-Pg boundary, which suggests a period of instability after the impact that is inferred to be the result of alternating conditions in soil that either favor aerobic or anaerobic bacteria, though more research is needed to validate this claim.
3. The hydrogen isotope measurements reflect isotopically light rain water that is depleted in deuterium, suggesting that the primary source of rain water was coming from the Pacific Ocean rather than the much more proximal Western Interior Seaway, as well as being influenced by a rain shadow effect and a relatively higher latitudinal placement to lower the $\delta^{2}H$ values of rain water.
4. The $\delta^{2}H$ values show a continuous decrease in the isotopic ratio which suggests that the Weatern Interior Seaway may still have contributed somewhat to the precipitation in the region but that its retreat was still recorded in the hydrogen isotopes of precipitation.
5. The carbon isotopic ratio shows a cyclic signal in the C_{25} and C_{29} lipid chains of 20-25,000 year intervals. This potential periodicity could be linked to precession Milankovitch cycles with the, however, the lack of a clear method of estimating rate of sedimentation means these measurements requires further investigation.
6. The evidence for Milankovitch cycles affecting the carbon isotopic composition of plant waxes but not bulk carbon suggests that these cycles were primarily affecting the plant

communities rather the carbon cycle being influenced by orbital cyclicity. It also shows that both sites had more localized effects with the different signal when comparing the C_{29} cycles between both sites.

7. A drastic shift in the ACL and Paq' from before to after the impact suggests a shift in the dominant plant types contributing to the plant wax record present, with aquatic plants being the primary contributors before the impact and terrestrial plants being the primary contributors after the impact.
8. The lack of an obvious signal at or above the K-Pg boundary from either site suggests that the carbon and water cycles had recovered from the initial disturbance brought upon from the extinction event within at most 16,000 years.

Contribution to knowledge

This thesis showcases the potential plant wax lipids provide as an application for studying the Cretaceous-Paleogene mass extinction and providing a way of studying the terrestrial carbon cycle in a way that has not been done before. Potential evidence of Milankovitch cycles affecting plant communities is novel for this time period and shows a strong affect that implies a relatively quick recovery after a devastating mass extinction. The hydrological cycle of the region is shown to be poorly understood and the mechanisms of the region need further investigation to better understand it. A high degree of instability in the bulk $\delta^{13}C$ record is seen after the impact which has not been noted in previous studies that more often focus on a smaller resolution.

Future directions

A lot has been gathered from this study that need to be investigated further. Most notably, the idea of Milankovitch cycles having an effect on terrestrial plant communities needs to be further investigated for this time period, with the sedimentation rate needing to be better defined to constrain the potential periodicity of these signals. Studying palynology over this time frame could prove useful in better understanding changing plant communities over the time scale of a couple hundred thousand years. Additionally, higher resolution sampling over the same intervals to better constraint changes in the cyclicity as well as having a stronger signal across the boundary to observe the immediate effect of the impact and extinction event on plant wax lipids would prove useful. Along with a higher resolution study, expanding the range well beyond the age observed could add additional information for long term changes both before the extinction event as well as in the earliest Paleocene.

The hydrological cycle needs further investigation as the highly depleted isotopic values are notable and will need stronger models to support the values that are recorded in the plant waxes. Links to the Deccan volcanism are weak with this study but can not be ruled out, and investigating links between the measurements collected and different models for Deccan volcanism could potentially provide a link between the two that we do not see by simply observing the trends.

References:

Aichner B., Herzschuh U., & Wilkes H. (2010). Influence of aquatic macrophytes on the stable carbon isotope signatures of sedimentary organic matter in lakes on the Tibetan Plateau. *Organic Chemistry*, 41, 706-718.

Alvarez L. W., Alvarez W., Asaro F., & Michel H. V. (1980). Extraterrestrial Cause for the Cretaceous-Tertiary Extinction. *Science*, 208, 1095-1108.

Arens N. C. & Jahren A. J. (2000). Carbon isotope excursion in Atmospheric CO_2 at the Cretaceous-Tertiary boundary: evidence from terrestrial sediments. *PALAIOS*, 15, 312-322.

Bamforth E. L., Button C. L., & Larsson H. C. E. (2014). Paleoclimate estimates and fire ecology immediately prior to the end-Cretaceous mass extinction in the Frenchman Formation (66 Ma), Saskatchewan, Canada. *Palaeogeography, Palaeoclimatology, Palaeoecology*, 401, 96-110.

Bowen G. J. and Revenaugh J. (2003). Interpolating the isotopic composition of modern meteoric precipitation. *Water Resources Research* **39**(10), 1299, doi:10.129/2003WR002086.

Bowen, G. J. (2019). The Online Isotopes in Precipitation Calculator, version 3.0. http://www.waterisotopes.org.

1292 Bradley R. S. (1988). The explosive volcanic eruption signal in northern hemisphere continental
1293 temperature records. *Climate Change*, 12, 221-243.
1294
1295 Catuneanu O. & Sweet A. R. (1999). Mastrichtian-Paleocene foreland-basin stratigraphies,
1296 western Canada: a reciprocal sequence architecture. *Canadian Journal of Earth Sciences*, 36,
1297 685-703.
1298
1299 Chiarenza A. A., Mannion P. D., Lunt D. J., Farnsworth A., Jones L. A., Kelland S. J., & Allison
1300 P. A. (2019). Ecological niche modelling does not support climatically-driven dinosaur diversity
1301 decline before the Cretaceous/Paleogene mass extinction. *Nature communications*. 10, 1091.
1302
1303 Clapham M. E. & Renne P. R. (2019). Flood basalts and mass extinctions. *Annual Review of*
1304 *Earth and Planetary Sciences*, 47, 275-303.
1305
1306 Croskell M., Warner M., & Morgan J. (2002). Annealing of shocked quartz during atmospheric
1307 re-entry. *Geophysical Research Letters*, 29, doi:10.1029/2001GL014382.
1308
1309 Dawson F.M., Evans C.G., Marsh R., Richardson R., Power B., Sweet A.R., & Edwards W.A.D.
1310 (1994). Uppermost Cretaceous and Tertiary Strata of the Western Canada Sedimentary Basin, in
1311 Geological Atlas of the Western Canada Sedimentary Basin. *Canadian Society of Petroleum*
1312 *Geologists and Alberta Research Council*, URL https://ags.aer.ca/publications/chapter-24-
1313 uppermost-cretaceous-and-tertiary-strata.
1314

D'Hondt S., Donaghay P., Zachos J. C., Luttenberg D., & Lindinger M. (1998). Organic carbon fluxes and ecological recovery from the Cretaceous-Tertiary mass extinction. *SCIENCE*, 282, 276-279.

Diefendorf A. F. & Freimuth E. J. (2017). Extracting the most from terrestrial plant-derived n-alkyl lipids and their carbon isotopes from the sedimentary record: A review. *Organic Geochemistry*, 103, 1-21.

Fastovsky D. E. & Bercovici A. (2016). The Hell Creek Formation and its contribution to the Cretaceous-Paleogene extinction: A short primer. *Cretaceous Research*, 57, 368-390.

Feng X. & Epstein S. (1994). Climatic implication of an 8000-year hydrogen isotope series from bristlecone pine trees. *Science*, 265, 1079-1081.

Ficken K. J., Li B., Swain D. L., & Eglinton G. (2000). An n-alkane proxy for the sedimentary input of submerged/floating freshwater aquatic macrophytes. *Organic Geochemistry*, 31, 745-749.

Font E., Adatte T., Sial A. N., de Lacerda L. D., Keller G., & Punekar J. (2016). Mercury anomaly, Deccan volcanism, and the end-Cretaceous mass extinction. *GEOLOGY*, 44, 171-174.

Harris D., Horwath W. R., & Kessel C. V. (2001). Acid fumigation of soils to remove carbonates prior to total organic carbon or carbon-13 isotopic analysis. *Soil Science Society of America Journal*, 65, 1853-1856.

Hildebrand A. R., Penfield G. T., Kring D. A., Pilkington M., Camargo A. Z., Jacobsen S. B., & Boynton W. V. (1991). Chicxulub Crater: A possible Cretaceous/Tertiary boundary impact crater on the Yucatán Peninsula, Mexico. *GEOLOGY*, 19, 867-871.

IAEA/WMO (2015). Global Network of Isotopes in Precipitation. The GNIP Database.

Imbrie J., Boyle E. A., Clemens S. C., Duffy A., Howard W. R., Kukla G., Kutzbach J., Martinson D. G., McIntyre A., Mix A. C., Molfino B., Morley J. J., Peterson L. C., Pisias N. G., Prell W. L., Raymo M. E., Shackleton N. J., & Toggweiler J. R. (1992). On the structure and origin of major glaciation cycles 1. Linear responses to Milankovitch forcing. *Paleoceanography*, 7, 701-738.

IPCC (2005). Special Report on Carbon Dioxide Capture and Storage. Prepared by Working Group III of the Intergovernmental Panel on Climate Change: Metz B, Davidson O, de Coninck HC, Loos M, Meyer LA (eds). Cambridge University Press, Cambridge, UK http://arch.rivm.nl/env/int/ipcc/ pages_media/SRCCS-fi nal/IPCCSpecial ReportonCarbon dioxideCaptureand Storage.htm

1358 Isaza-Londoño C., MacLeod K. G., & Huber B. T. (2006). Maastrichtian North Atlantic
1359 warming, increasing stratification, and foraminiferal paleobiology at three timescales.
1360 *Paleoceanography*, 21, PA1012, doi:10.1029/2004PA001130
1361
1362 Ittekkot V. (1993). The abiotically driven biological pump in the ocean and short-term
1363 fluctuations in atmospheric CO_2 contents. *Global and Planetary Change*, 8, 17-25.
1364
1365 Ivanov B. A. (2005). Numerical modeling of the largest terrestrial meteorite craters. *Solar*
1366 *System Research*, 39, 381-409.
1367
1368 Jerrett R. M., Price G. D., Grimes S. T., & Dawson A. T. (2015). A paleoclimate and
1369 paleoatmospheric record from peatlands accumulating during the Cretaceous-Paleogene
1370 boundary event, Western Interior Basin, Canada. *GSA Bulletin*, 127, 1564-1582.
1371
1372 Kaiho K., Kajiwara Y., Tazaki K., Ueshima M., Takeda N., Kawahata H., Arinobu T., Ishiwatari
1373 R., Hirai A., & Lamolda M. A. (1999). Oceanic primary productivity and dissolved oxygen
1374 levels at the Cretaceous/Tertiary boundary: Their decrease, subsequent warming, and recovery.
1375 *Paleoceanography*, 47, 511-524.
1376
1377 Keeley J. E. & Sandquist D. R. (1992). Carbon: freshwater plants. *Plant, Cell, and Environment*,
1378 15, 1021-1035.
1379

1380 Khadkikar A. S., Sant D. A., Gogte V., & Karanth R. V. (1999). The influence of Deccan
1381 volcanism on climate: insights from lacustrine intertrappean deposits, Anjar, western India.
1382 *Palaeogeography, Palaeoclimatology, Palaeoecology*, 147, 141-149.
1383
1384 Kolattukudy P. E. (1969). Plant Waxes[1]. Symposium on Natural Waxes.
1385
1386 Kring D. A. & Durda D. D. (2002). Trajectories and distribution of material ejected from the
1387 Chicxulub impact crater: Implications for postimpact wildfires. *Journal of Geophysical*
1388 *Research*, 107, 10.1029/2001JE001532.
1389
1390 Kupsch W. O. (1957). Frenchman Formation of Eastern Cypress Hills, Saskatchewan, Canada.
1391 *Bulletin of the Geological Society of America*, 68, 413-420.
1392
1393 Labandeira C. C., Johnson K. R., & Lang P. (2002). Preliminary assessment of insect herbivory
1394 across the Cretaceous-Tertiary boundary: Major extinction and minimal rebound. *Geological*
1395 *Society of America Special Paper*, 361, 297-327.
1396
1397 Lehman T. M. (1989). Upper Cretaceous (Maastrichtian paleosols in Trans-Pecos, Texas.
1398 *Geological Society of America Bulletin*, 101, 188-203.
1399
1400 Liu H., Liu Z., Zhao C., & Liu W. (2019). n-Alkyl lipid concentrations and distributions in
1401 aquatic plants and their individual δD variations. Science China Earth Science, 62,
1402 https://doi.org/10.1007/s11430-019-9370-8

Lomax B., Beerling D. Upchurch G Jr, & Otto-Bliesner B. (2001). Rapid (10-yr) recovery of terrestrial productivity in a simulation study of the terminal Cretaceous impact event. *Earth and Planetary Science Letters*, 192, 137-144.

MacLeod K. G., Huber B. T., Pletsch T., & Röhl U. (2001). Maastrichtian foraminiferal and paleoceanographic changes on Milankovitch timescales. *Paleoceanography*, 16, 133-154.

Maruoka T., Koerberl C., & Bohor B. F. (2007). Carbon isotopic compositions of organic matter across continental Cretaceous–Tertiary (K-T) boundary sections: Implications for paleovenvironment after the K-T extinction event. *Earth and Planetary Science Letters*, 253, 226-238.

Mason E., Edmonds M., & Turchyn A. V. (2017). Remobilization of crustal carbon may dominate volcanic arc emissions. *Science*, 357, 290-294.

Meyers P. A. & Simoneit B. R. T. (1990). Global comparisons of organic matter in sediments across the Cretaceous/Tertiary boundary. *Organic Geochemistry*, 16, 641-648.

Meyers P.A. (1994). Preservation of elemental and isotopic source identification in sedimentary organic matter. *Chemical Geology*, 114, 289-302.

McIver E. E. (1989). Fossil Flora of the Paleocene Ravenscrag Formation, Southwestern Saskatchewan, Canada. *University of Saskatchewan*.

McIver E. E. (2002). The paleoenvironment of *Tyrannosaurus rex* from southwestern Saskatchewan, Canada. *Canadian Journal of Earth Sciences*, 39, 207-221.

Miller K. G., Barrera E., Olsson R. K., Sugarman P. J., & Savin S. M. (1999). Does ice drive Maastrichtian eustasy? *Geology*, 27, 783-786.

Mook W.G., Bommerson J.C. and Staverman W.H. (1974) Carbon isotope fractionation between dissolved bicarbonate and gaseous carbon dioxide. *Earth and Planetary Science Letters*, 22, 169-176.

Natelhoffer K. J. & Fry B. (1988). Controls on natural nitrogen-15 and carbon-13 abundances in forest soil organic matter. *Soil Society of America Journal*, 52, 1633-1640.

Norris R. D., Huber B. T., & Self-Trail J. (1999). Synchroneity of the K-T oceanic mass extinction and the meteorite impact: Blake Nose, western North Atlantic. *Geology*, 27, 419-422.

Osborne C. P. & Beerling D. J. (2005). Nature's green revolution: the remarkable evolutionary rise of C_4 plants. *Philosophical Transactions of Royal Society B*, 361, 173-194.

1447 Petersen S. V., Dutton A., & Lohmann K. C. (2016). End-Cretaceous extinction in Antarctica
1448 linked to both Deccan volcanisms and meteorite impact via climate change. *Nature*
1449 *Communications*, DOI: 10.1038/ncomms12079.
1450
1451 Pope K. O., Baines K. H., Ocampo A. C., & Ivanov B. A. (1994). Impact winter and the
1452 Cretaceous/Tertiary extinctions: Results of a Chicxulub asteroid impact model. *Earth and*
1453 *Planetary Science Letters*, 128, 719-725.
1454
1455 Pope K. O., Baines K. H., Ocampo A. C., & Ivanov B. A. (1997). Energy, volatile production,
1456 and climate effects of the Chicxulub Cretaceous/Tertiary impact. *Journal of Geophysical*
1457 *Research*, 102, 21,645-21,664.
1458
1459 Prinn R. G. & Fegley Jr. B. (1987). Bolide impact, acid rain, and biospheric traumas at the
1460 Cretaceous-Tertiary boundary. *Earth and Planetary Science Letters*, 83, 1-15.
1461
1462 Redman C. M., Gardner J. D., Scott C. S., & Braman D. R. (2015). Geological setting of
1463 vertebrate microfossil localities across the Cretaceous-Paleogene boundary in southwestern
1464 Saskatchewan, Canada. *Canadian Journal of Earth Sciences*, 52, 846-862.
1465
1466 Renne P. R., Deino A. L., Hilgen F. J., Kuiper K. F., Mark D. F., Mitchel III W. S., Morgan L.
1467 E., Mundil R., & Smit J. (2013). Time scales of critical events around the Cretaceous-Paleogene
1468 boundary. *SCIENCE*, 339, 684-687.
1469

1470 Sachse D., Billault I., Bowen G. J., Chikaraishi Y., Dawson T. E., Feakins S. J., Freeman K. H.,
1471 Magill C. R., McInerney F. A., van der Meer M. T. J., Polissar P., Robins R. J., Sachs J. P.,
1472 Shmidt H. L., Sessions A. L., White J. W. C., West J. B., & Kahmen A. (2012). Molecular
1473 Paleohydrology: Interpreting the Hydrogen-Isotopic Composition of Lipid Biomarkers from
1474 Photosynthesizing Organisms. *Annual Review of Earth and Planetary Sciences*, 40, 221-249.
1475
1476 Saward S. A. (1992). A global view of Cretaceous vegetation patterns. *Geological Society of*
1477 *America Special Paper*, 267, 17-35.
1478
1479 Saxena V. K., Yu S., & Anderson J. (1997). Impact of stratospheric volcanic aerosols on climate:
1480 evidence for aerosol shortwave and longwave forcing in the southeastern U.S. *Atmospheric*
1481 *Environment*, 31, 4211-4221.
1482
1483 Schoene B., Eddy M. P., Samperton K. M., Keller C. B., Keller G., Adatte T., & Khadri S. F. R.
1484 (2019). U-Pb constraints on pulsed eruption of the Deccan Traps across the End-Cretaceous mass
1485 extinction. *Science*, 363, 862-866.
1486
1487 Sepúlveda J., Alegret L., Thomas E., Haddad E., Cao C., & Summons R. E. (2019). American
1488 Geophysical Union.
1489
1490 Sharp Z. D. (2007). Principles of Stable Isotope Geochemistry. Prentice Hall, New York, 360 pp.
1491

Sheehan P. M., Fastovsky D. E., Barreto C., & Hoffmann R. G. (2000). Dinosaur abundance was not declining in a "3 m gap" at the top of the Hell Creek Formation, Montana and North Dakota. *Geology*, 28, 523-526.

Smit J. & Hertogen J. (1980). An extraterrestrial event at the Cretaceous-Tertiary boundary. *Nature*, 285, 198-200.

Spicer, R. A. and Herman, A. B. (2010). The late Cretaceous environment of the Arctic: A quantitative reassessment based on plant fossils. Palaeogeography, Palaeoclimatology, Palaeoecology, 295, 423–442.

Sprain C. J., Renne P. R., Vanderkluysen L., Pande K., Self S., & Mittal T. (2019). The eruptive tempo of Deccan volcanism in relation to the Cretaceous-Paleogene boundary. *Science*, 363, 866-870.

Super J. R., Chin K., Pagani M., Li H., Tabor C., Harwood D. M., & Hull P. M. (2018). Late Cretaceous climate in the Canadian Arctic: Multi-proxy constraints from Devon Island. *Palaeoceanography, Palaeoclimatology, Palaeoecology*, 504, 1-22.

Sweet A. R., Braman D. R., & Lerbekmo J. F. (1999). Sequential palynological changes across composite Cretaceous-Tertiary (K-T) boundary claystone and contiguous strata, western Canada and Montana, U.S.A. *Canadian Jouranl of Earth Sciences*, 36, 743-768.

1515 Swenson N. G. & Enquist B. J. (2007). Ecological and evolutionary determinants of a key plant
1516 functional trait: Wood density and its community-wide variation across latitude and elevation.
1517 *American Journal of Botany*, 94, 451-459.
1518
1519 Therrien F., Eberth D. A., Braman D. R., & Zelenitsky (2007). High-resolution organic carbon
1520 isotope record across the Cretaceous-Tertiary boundary in south-central Alberta: implications for
1521 the post-impact recovery rate of terrestrial systems and use of $\delta^{13}C$ as a boundary marker.
1522 *Canadian Journal of Earth Sciences*, 44, 529-542.
1523
1524 Vajda V., Raine J. I., & Hollis C. J. (2001). Indication of global deforestation at the Cretaceous-
1525 Tertiary boundary be New Zealand fern spike. *Science*, 294, 1700-1702.
1526
1527 Vellekoop J., Sluijs A., Smit J., Schouten S., Weijers J. W. H., Sinninghe Damsté J. S., &
1528 Brinkhuis H. (2014). Rapid short-term cooling following the Chicxulub impact at the
1529 Cretaceous-Paleogene boundary. *PNAS*, 111, 7537-7541.
1530
1531 Vellekoop J., Smit J., Schootbrugge B., Weijers J. W. H., Galeotti S., Sinninghe Damsté J.S., &
1532 Brinkhuis H. (2015). Palynological evidence for prolonged cooling along the Tunisian
1533 continental shelf following the K-Pg boundary impact. *Palaeogeography, Palaeoclimatology,*
1534 *Palaeoecology*, 426, 216-228.
1535
1536 Vermeer M. & Rahmstorf S. (2009). Global sea level linked to global temperature. *PNAS*, 106,
1537 21527-21532.

Walls R. A., Mountjoy E. W., & Fritz P. (1979). Isotopic composition and diagenetic history of carbonate cements in Devonian Golden Spike reef, Alberta, Canada. *Geological Society of America Bulletin*, 90, 963-982.

Washington H. S. (1922). Deccan traps and other plateau basalts. *Bulletin of the Geological Society of America*, 33, 765-804.

Westerhold T., Röhl U., Raffi I., Fornaciari E., Monechi S., Reale V., Bowles J., & Evans H. F. (2008). Astronomical calibration of the Paleocene time. *Palaeogeography, Palaeoclimatology, Palaeoecology*, 257, 377-403.

Wilf P., Johnson K. R., & Huber B. T. (2003). Correlated terrestrial and marine evidence for global climate changes before mass extinction at the Cretaceous-Paleogene boundary. *PNAS*, 100, 599-604.

Willis K. J., Kleckowski A., & Crowhurst S. J. (1999). 124,000-year periodicity in terrestrial vegetation change during the late Pleistocene epoch. *Nature*, 397, 685-688.

Willis K. J. & Niklas K. J. (2004). The role of Quaternary environmental change in plant macroevolution: the exception of the rule? *Philosophical Transactions of the Royal Society of London*, 359, 159-172.

Wolfe J. A. & Upchurch Jr. G. R. (1986). Vegetation, climactic, and floral changes at the Cretaceous-Tertiary boundary. *Nature*, 324, 148-152.

Yamamoto S., Hasegawa T., Tada R., Goto K., Rojas-Consuegra R., Díaz-Otero C., García-Delgado D. E., Yamamoto S., Sakuma H., & Matsui T. (2010). Environmental and vegetational changes recorded in sedimentary leaf wax n-alkanes across the Cretaceous-Paleogene boundary at Loma Capiro, Central Cuba. *Palaeogeography, Palaeoclimatology, Palaeoecology*, 295, 31-41.